Hui Guo[a,b,c], Hui Sun[a], Fanhao Meng[a,*], Chula Sa[a], Min Luo[a]

a College of Geographical Science, Inner Mongolia Normal University, Hohhot 010022, China

b Department of Water Conservancy Engineering, North China University of Water Conservancy and Electric Power, Zhengzhou 450046, China

c State Key Laboratory of Hydroscience and Engineering, Department of Hydraulic Engineering, Tsinghua University, Beijing 100084, China

* Correspondence author. Fanhao Meng (mfh320@imnu.edu.cn)

Hui Guo and Hui Sun contributed equally to this work

Key Points:

- Compared with CMIP5, the comprehensive simulation ability of the BCC, CCCma, NCAR, CAS, MIP-M and NCC models in CMIP6 has been improved.
- The multi-model ensemble mean has better performance than most individual model simulations for CMIP5 and CMIP6.
- The decline in spring SCF is inconsistent between emission scenarios, with the most pronounced decline in the high emission scenario.

Abstract

Assessment of spring snow cover fraction (SCF) can be valuable for understanding the efficacy of certain Earth system models (ESMs) in simulating the energy exchange between land and atmosphere system, global hydrological cycle and future climate impacts. In this work, we studied the model performance of 23 and 20 ESMs participating CMIP5 and CMIP6 by comparing satellite data from National Oceanic and Atmospheric Administration and National Climatic Data Center (NOAA/NCDC) over the Northern Hemisphere (NH) and its 13 sub-regions and evaluated potential model improvement from CMIP5 to CMIP6 and predicted spring SCF in the future. We found that the mean annual spring SCF that was simulated by CMIP5 and CMIP6 models was underestimated in most of the NH and overestimated on the Tibetan Plateau and in eastern Asia, and most of the model simulations showed a stronger reduction trend as well as an underestimated monthly climatological SCF. However, compared with those in CMIP5, most of the model simulations in CMIP6 had an improved ability to simulate spring SCF in terms of the annual mean, long-term trend and intra-annual variability. We also confirmed that the multi-model ensemble mean (MME) is a better way to represent the three aspects of spring SCF than most individual model simulations. The spring SCF values predicted by the CMIP5 and CMIP6 MMEs over the NH and its 13 sub-regions under different scenarios showed decreasing trends. The decreasing spring SCF trends differed

under different scenarios, and the SCF under high emissions scenarios (RCP 8.5 and SSP5-8.5) continued to decrease.

1 Introduction

Snow, as an important part of the cryosphere, is the most sensitive element to climate change. Due to its unique radiative (high surface albedo) and thermal (low thermal conductivity) properties, a small variation in snow cover can substantially af-fect the energy budget of the land-atmosphere system and then climate change (Qu & Hall, 2005; Euskirchen et al., 2007; Trenberth & Fasullo, 2009; Flanner et al., 2011; Groisman et al., 2017; Kang et al., 2019). Meanwhile, snow is also an important freshwater resource and an indispensable part of the hydrological cycle (Stewart et al., 2004; Barnett et al., 2005; Barnhart et al., 2016; Sturm et al., 2017). With climate change, snow cover has shown significant decreasing trends during the few past decades over the Northern Hemisphere (NH), especially in the spring season (Déry & Brown, 2007; Brown et al., 2010; Brown & Robinson, 2011; Derksen & Brown, 2012; Brutel-Vuilmet et al., 2013; Brown et al., 2017; Meredith et al., 2019). This decline in the spring snow cover fraction (SCF) has been related to the mean local climate. Some researchers have demonstrated that there is a spring snow-albedo feedback mechanism induced by snow cover changes over the NH (e.g., Fernandes et al., 2009; Flanner et al., 2011), and these studies showed that the positive spring snow–albedo feedback through the reduction of snow cover plays an essential role in accelerating global or regional temperature (e.g., Hall. 2004; Winton, 2006; Pithan et al., 2014). Therefore, given the important impact of spring snow cover changes on climate, the evolution and possible changes in spring SCF historically and in the future is a matter of concern.

At present, the state-of-the-art Earth System Models (ESMs) participating in the Coupled Model Intercomparison Projects (CMIPs) are important tools for conducting research on the climate change. However, ESMs have been introduced substantial un-certainties in estimating SCF (Bormann et al., 2018; Mudryk et al., 2015). Evaluating the performance of ESM outputs in the simulation of spring SCF is therefore essential to gain greater confidence in scientific research or policies. Many efforts have been made to evaluate the performance of the ESM outputs of SCF from CMIP3 and CMIP5 at global and regional scales (e.g., Brutel-Vuilmet et al., 2013; Hardiman et al., 2008; Zhu & Dong, 2013; Furtado et al., 2015; Li et al., 2016; Santolaria-Otín & Zolina, 2020). These studies provide valuable references for a rapid understanding of historical and future global and regional snow cover changes, and they have shown that both the CMIP3 and CMIP5 models tend to underestimate the trend of decreasing spring snow cover compared to observed datasets (Derksen & Brown, 2012; Flanner et al., 2009; Frei et al., 2003). For example, Zhu & Dong (2013) found that most model simulations in CMIP5 underestimate the trend of snow reduction in March-April over the NH compared with the NH EASE Grid 2.0 Weekly Snow Cover and Sea Ice Extent dataset. Moreover, the lack of significant improvement in the ability of CMIP5 to simulate snow cover relative to

the CMIP3 model (Xia & Wang, 2015) may be related to the model's structure and parameters (Wang et al., 2016; Thackeray et al., 2015; Loranty et al., 2014). With the advent of the CMIP, the CMIP6 outputs have a higher spatial resolution and improved parameterization schemes for physical process (Taylor et al., 2012; Eyring et al., 2016), and its scientific combination of shared socioeconomic pathways (SSPs) and representative concentration pathways (RCPs) scenarios incorporating the impacts of socio-economic development provides a more reliable picture of likely climate change outcomes. Zhu et al. (2021) evaluated the historical evolution of snow cover over the NH using CMIP5 and CMIP6 models according to observation datasets and future trends. Mudryk et al. (2020) analysed observed and simulated historical snow cover extent and snow mass as well as future snow cover projections from CMIP6. In addition, the CMIP6 output was compared to CMIP5 results to assess the progress between these two successive model generations. Previous studies employed different performance metrics to assess the ability of these two generations of models to simulate SCF while still lacking integrated metrics that can help researchers intuitively determine whether CMIP6 has a better simulation performance than CMIP5. Moreover, few studies have been devoted to assessing the ability of these two generations of models to simulate historical SCF and predict future snow cover changes at regional scales under different emission scenarios, which greatly impedes the prognosis of ecological and water resources, among others, at regional scales and the science of developing corresponding climate change policies for adaptation to climate change.

To fill this gap, this study aims to (i) evaluate these two generations of models in reproducing spring SCF over the NH and its different areas through annual mean, long-term trends, and intra-annual variabilities against observation datasets according to multiple metrics; (ii) decide whether CMIP6 models can simulate snow cover changes better than CMIP5 models when using an integrated metric at global and regional scales; and (iii) determine the evolution trend of snow cover changes over the NH and its dif-ferent regions under different future RCPs and SSPs as projected by the CMIP5 and CMIP6 models. The results of this study could provide valuable scientific references to end-users of CMIP5 and CMIP6 SCF simulations for their particular applications at different spatial scales.

2 Materials and Methods

2.1 Observational data

For the observational SCF dataset, we adopted the NH EASE Grid 2.0 Weekly Snow Cover and Sea Ice Extent dataset (Robinson et al., 1993; Brodzik & Armstrong, 2013) from the National Oceanic and Atmospheric Administration and National Climatic Data Center (NOAA/NCDC) (hereafter referred to as the NOAA dataset), since the NOAA SCF was quality-controlled by the cartographer's hand drawing before 1996 and validated by the MODIS/Terra snow cover L3 dataset (MOD10A1, version 6) during their overlapping period (i.e., from 2000-2005) (Coll and Li, 2018). The monthly SCF is derived by averag-

ing weekly snow cover extent in which signed by 1 value (i.e., 50% or larger probability of snow occurrence). Considering historically CMIP5 output data is available up to 2005, the period of 1982-2005 is taken as the his-torical baseline in this paper.

2.2 Climate gridded datasets

Monthly temperature and precipitation data at a spatial resolution of 0.5°×0.5° covering the period 1982-2005 are obtained from the Climate Research Unit gridded Times Series, version 4 (CRU TS, 4.04) (Harris et al., 2020). This dataset was interpo-lated from over 4000 meteorological station records over the NH and has been widely used to investigate climate change around the world (e.g., Bellprat et al., 2019; Chen et al., 2015; Kannenberg et al., 2019). The CRU data were selected as the benchmark to assess the ability of ESMs to simulate near-surface temperature and precipitation.

2.3 Climate model simulations

Outputs of climate models participating in CMIP5 (Taylor et al., 2012) and CMIP6 (Eyring et al., 2016) experiments are used here to investigate spring SCF changes in model simulations during historical (1982-2005) and future (2006-2099) periods. For future simulations in CMIP5, we use RCPs at three different levels of forcing (RCP 2.6, RCP 4.5 and RCP 8.5) (Meinshausen et al., 2011). The CMIP6 provides a richer set of global climate model outputs, and its scientific combination of SSP and RCP scenarios that incorporate the impacts of socio-economic development provide a more reliable picture of likely climate change outcomes. In this study, we adopt the SSP1-2.6, SSP2-4.5 and SSP5-8.5 scenarios for the CMIP6 experiment. We obtain monthly outputs of monthly SCF, near-surface air temperature, and precipitation in historical (1982-2005) and future (2006-2099) periods from 23 CMIP5 models and 20 CMIP6 models (Table S1 in Supporting Information S1). Most models have multiple realizations, while few models only have one. Considering that the ensemble means of a large number of realizations will increase variability across models, we use only the first realization (r1i1p1 and r1i1p1f1, respectively) in all CMIP5 and CMIP6 models. All model outputs are resampled to a 0.25° spatial resolution using the first-order conservative method (Jones, 1999; https://code.zmaw.de/projects/cdo).

2.4 Evaluation metrics methods

In the present study, the SCF accuracy from CMIP5 and CMIP6 over the NH and its 13 sub-regions during the historical period is evaluated from three aspects: the annual mean spring SCF, long-term trend, and intra-annual variability. First, the annual mean spring SCF is evaluated based on the Taylor diagram and Taylor skill score (TSS); second, relative bias (RB) is used to test the accuracy of the long-term trend of spring SCF; third, three indicators (bias, root mean square error (RMSE) and correlation coefficient (r)) are used to evaluate the intra-annual variability of spring SCF, and then these three statistics are combined into a comprehensive rating index (CRI) to rank the model's

ability to simulate the intra-annual variability of spring SCF (CRIac). Fourth, TSS, RB, and CRIac are used to calculate the CRI to provide a comprehensive performance score for the models in simulating spring SCF. The details of the methods are as follows.

2.4.1 Taylor Diagram and Taylor Skill Score

The Taylor diagram (Taylor, 2001) is used to assess the ability of the ESMs to capture the spatial pattern of the SCF. The Taylor diagram can summarize the three statistics of r, RMSE and the normalized standard deviation (SD) in one graph. Among these statistics, a larger r value, a smaller RMSE and a SD that is close to 1 all indicate that the spatial pattern characteristics of the spring SCF that are simulated by the models are closer to the observational data.

To quantitatively characterize the model's simulation ability, the TSS is used to assess each model's ability to simulate SCF across the NH and its 13 sub-regions, according to the methods of Taylor (2001). The TSS is calculated by the following equation:

$$TSS = \frac{4(1+r)^2}{\left(\frac{\sigma_o}{\sigma_m}+\frac{\sigma_m}{\sigma_o}\right)^2(1+r_0)^2} \quad (1)$$

where r is the spatial correlation coefficient between the model and the observational data, and σ_o and σ_m are the standard deviations of the observed data and model simulations, respectively. The value of TSS ranges from 0 to 1, where values closer to 1 indicate better performance in simulating the spatial pattern of spring SCF.

2.4.2 Relative bias

To measure the proximity of the ESMs trend to the observational trend, the relative bias (RB) of the trend slope is calculated based on the following equation:

$$RB = \frac{S_m - S_o}{S_o} \quad (2)$$

where Sm and So denote the long-term trend of the model simulations and the observational data, respectively. The closer the value of RB is to 0, the better the performance of the ESMs in simulating the long-term trend of spring SCF.

2.4.3 Intra-annual variability evaluation indicators

The ability of different models to simulate the intra-annual variability of spring SCF is mainly assessed by three statistical indicators: bias, RMSE and r. Among these indicators, bias is used to measure the difference in the intra-annual variability of spring SCF between the ESMs and the observational data. The RMSE is used to measure the degree of dispersion of the ESMs against the

observational data. In addition, r is used to describe the correlation between the ESMs and the observational data. These three statistical indicators are calculated from the climatological monthly SCF in spring (March-May) with the following equations:

$$Bias = \frac{1}{N}\sum_{i=1}^{N}(M_i - O_i) \quad (3)$$

$$RMSE = \sqrt{\frac{1}{N}\sum_{i=1}^{N}(M_i - O_i)^2} \quad (4)$$

$$r = \frac{\mathrm{Cov}(M,O)}{\sigma M \bullet \sigma O} \quad (5)$$

where M denotes the ESMs; O denotes the observational data; "Cov" denotes the covariance, which is used to measure the overall error between two variables; and denotes the standard deviation. The closer the values of the bias and RMSE are to 0, the better the model simulation results; the values of r range from -1 to 1, and the closer r is to 1, the higher the correlation between the ESMs and the observational data.

2.4.4 Comprehensive rating index

The CRI is currently widely used to rank the simulation ability of ESMs (e.g., Jiang et al., 2015; Zhang et al., 2018; Guo et al., 2021). Here, the CRI is first used to provide the CRIac of the intra-annual variability of spring SCF by combining three indicators (bias, RMSE and r), and then it is used to rank the overall performance of each ESM through TSS, RB and CRIac. The equation for calculating the CRI is as follows:

$$CRI = 1 - \frac{1}{\mathrm{nm}}\sum_{i=1}^{n}\mathrm{rank}_i \quad (6)$$

where n is the number of indices used to evaluate model performance and m is the total number of ESMs and the multi-model ensemble mean (MME). The model with the best performance is assigned a rank value of 1. Therefore, the closer to 1 the value of CRI is, the better the model performs.

3 Results

3.1 Assessment of spring SCF simulated by ESMs during the historical period

3.1.1 Spatial pattern of the annual mean spring SCF

We first evaluate the spatial pattern of the annual mean spring SCF (March-May) bias between the model simulations and NOAA data (Figure 1, Figure 2). Generally, there are negative bias between model simulations from CMIP5 and CMIP6 and NOAA annual mean spring SCF in most regions, especially in the Alaska/N. W Northwest Canada region (ALA; region #2 in Figure 3) and in Central Asia (CAS; region #12 in Figure 3). Positive bias is shown in the Tibetan Plateau (TIB; region #13 in Figure 3) and East Asia (EAS; region #14

in Figure 3). For example, the bias values of the CMIP5 (CMIP6) models in the ALA and CAS regions are -17.51±16.86% (-16.16±15.85%) and -11.60±6.35% (-9.36±8.58%), respectively, and they are 16.69±13.32% (16.55±13.26%) and 6.71±5.96% (6.16±5.96%) in the TIB and EAS regions, respectively. However, the spatial pattern of the annual mean spring SCF from MME simulations has a better performance than most individual models. For example, for the TIB region, 2/3 of the CMIP5 and CMIP6 model simulations have absolute values of bias greater than those of the CMIP5 MME (7.76) and CMIP6 MME (4.45). It should be noted that the spatial pattern of the annual mean spring SCF relative bias from the CMIP6 MME shows an improvement over the CMIP5 MME. For example, the simulated spring SCF in the CMIP6 MME across the NH is closer to the NOAA data than the CMIP5 MME is, with biases of -2.41 and -4.45, respectively.

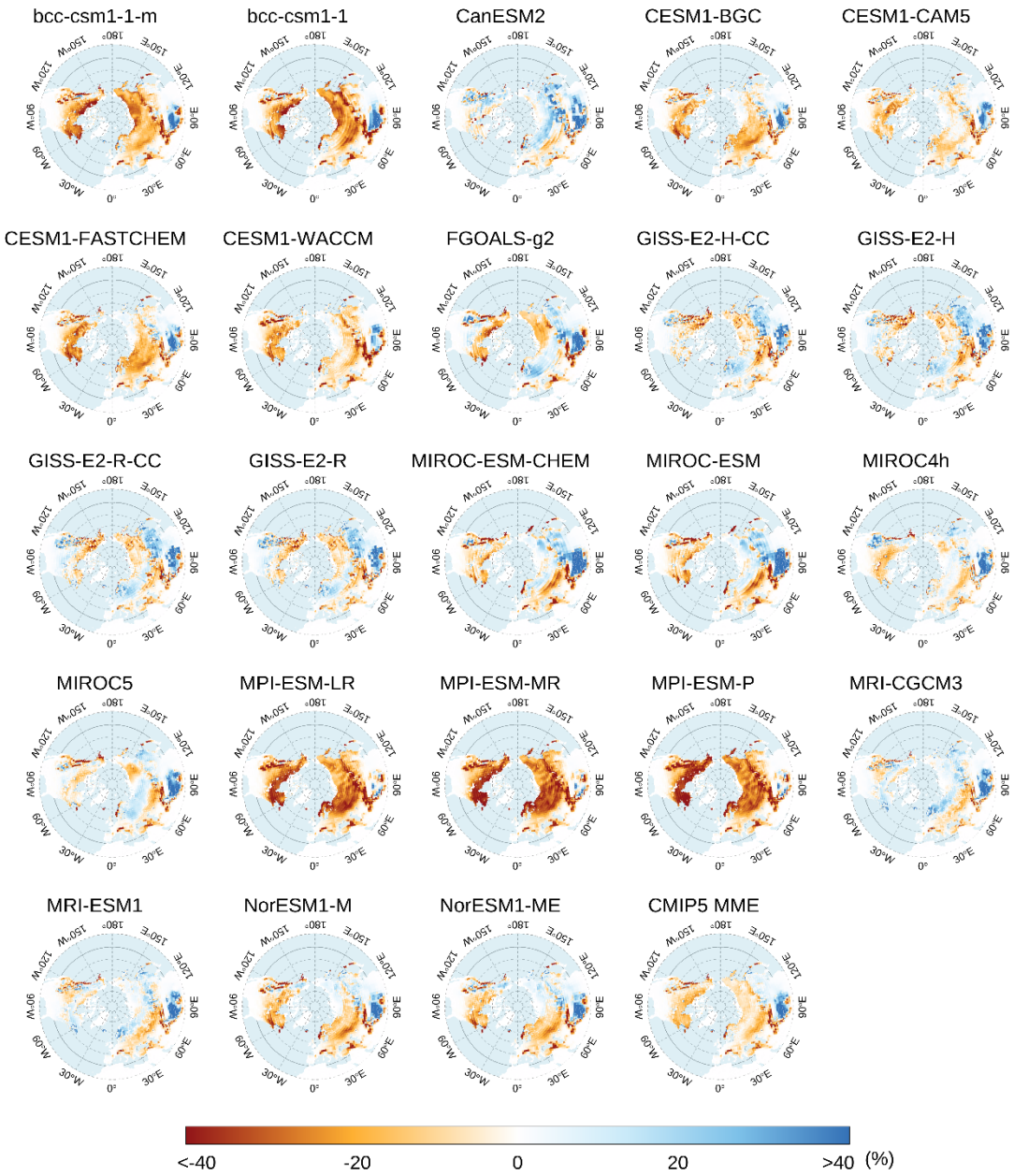

Figure 1. Spatial pattern of the annual mean spring (March, April and May) SCF relative bias between the NOAA data and CMIP5 model simulations as well as the CMIP5 MME over the NH during the period of 1982-2005.

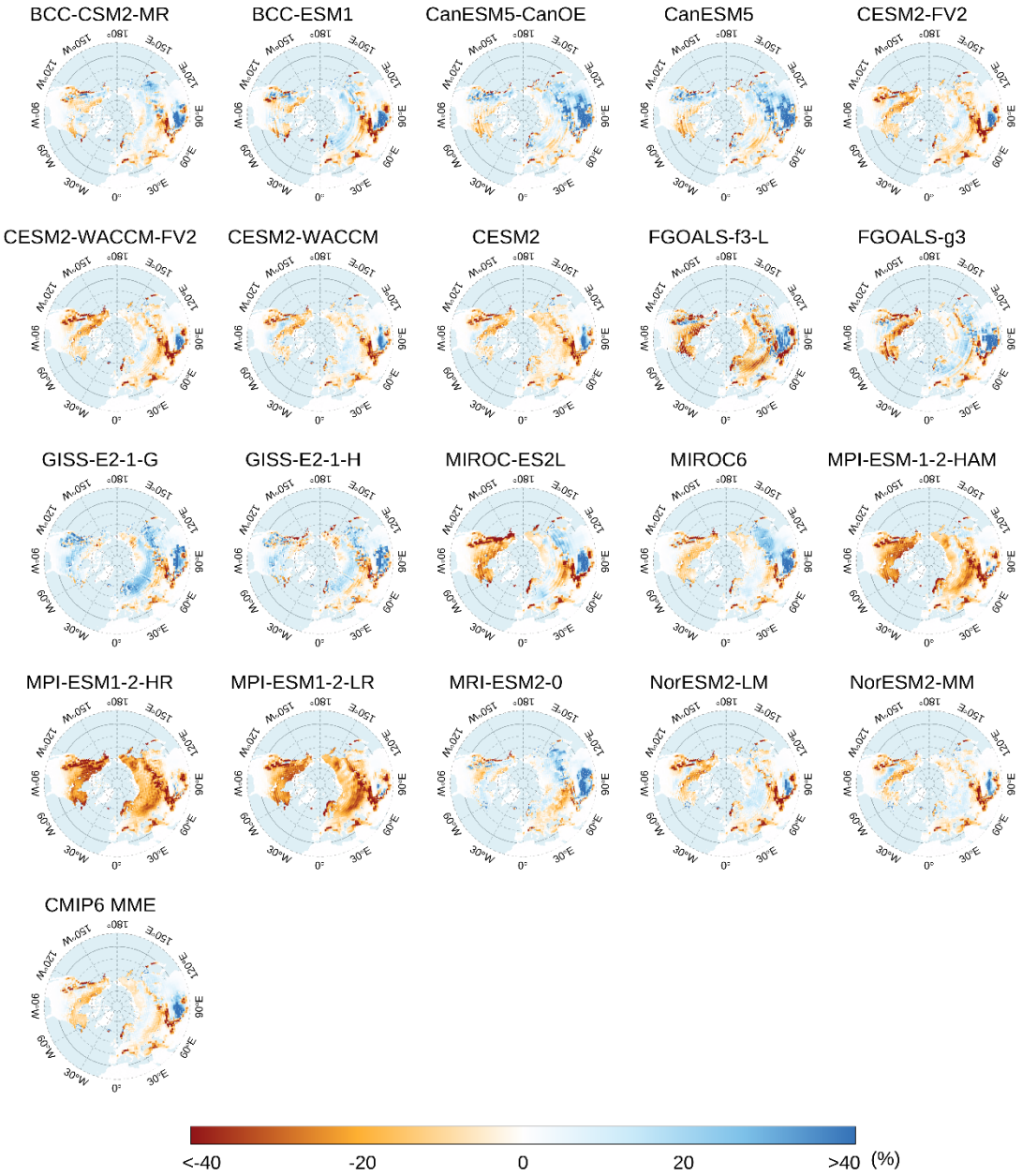

Figure 2. Spatial pattern of the annual mean spring (March, April and May) SCF relative bias between the NOAA data and CMIP6 model simulations as well as the CMIP6 MME over the NH during the period of 1982-2005.

Next, we use the Taylor diagram and the TSS to measure how well each model simulation from the CMIP5 (Figure 3) and CMIP6 (Figure 4) models approxi-

mate the annual mean spring SCF over the NH and its 13 sub-regions.

Broadly, the r between each model's simulations (CMIP5 and CMIP6) and their MMEs and the NOAA data ranges from 0.8 to 0.95, the SD is concentrated at approx-imately 1 (Figure 3, Figure 4), and the TSSs are greater than 0.94 (Table S2 and Table S3 in Supporting Information S1). This indicates that each model simulation of the CMIP5 and CMIP6 models and their MMEs can better simulate the spatial pattern of the annual mean spring SCF over the NH. We then divide the NH into 13 sub-regions, and the spatial pattern of the annual mean spring SCF in different regions clearly shows large variations across model simulations compared to the NOAA data (Figure 3 and Figure 4). In ALA, South Europe/Mediterranean (MED; region #9 in Figure 3), West Asia (WAS; region #11 in Figure 3) and TIB, the r values between all CMIP5 and CMIP6 model simulations and the NOAA data are small (-0.24-0.76), the SD values are more spread out (0.01-2.4), and the TSS values are less than 0.85. However, the TSS value in North Asia (NAS; region #10 in Figure 3) is significantly larger than that in the remaining regions, with r ranging from 0.71 to 0.90, and a SD of approximately 1. For MME, the CMIP5 and CMIP6 MMEs have better performance in West North America (WNA; region #3 in Figure 3), Central North America (CNA; region #5 in Figure 3), East North America (ENA; region #6 in Figure 3), North Europe (NEU; region #7 in Figure 3), NAS and EAS, with TSS values greater than 0.96, r values greater than 0.83 and SD values between 0.75-1.02. While the MMEs have a limited performance in the MED, WAS, and TIB regions, with TSS values less than 0.84, the r values range from 0.38-0.79 and the SD values range from 0.14-0.94. In particular, the worst performance was found in the MED region (TSS values of 0.49 and 0.52 for the CMIP5 and CMIP6 MMEs, respectively). Com-pared with the CMIP5 MME, the SD values of the CMIP6 MME are closer to 1, and the TSSs are larger (Table S2 and Table S3 in Supporting Information S1) in the Canada/not include Greenland/Iceland (CGI; region #4 in Figure 3), CNA, ENA, Central Europe (CEU; region #8 in Figure 3), MED, WAS, and EAS regions, indicating the improved ability of the CMIP6 MME to simulate the annual mean spring SCF in these seven regions.

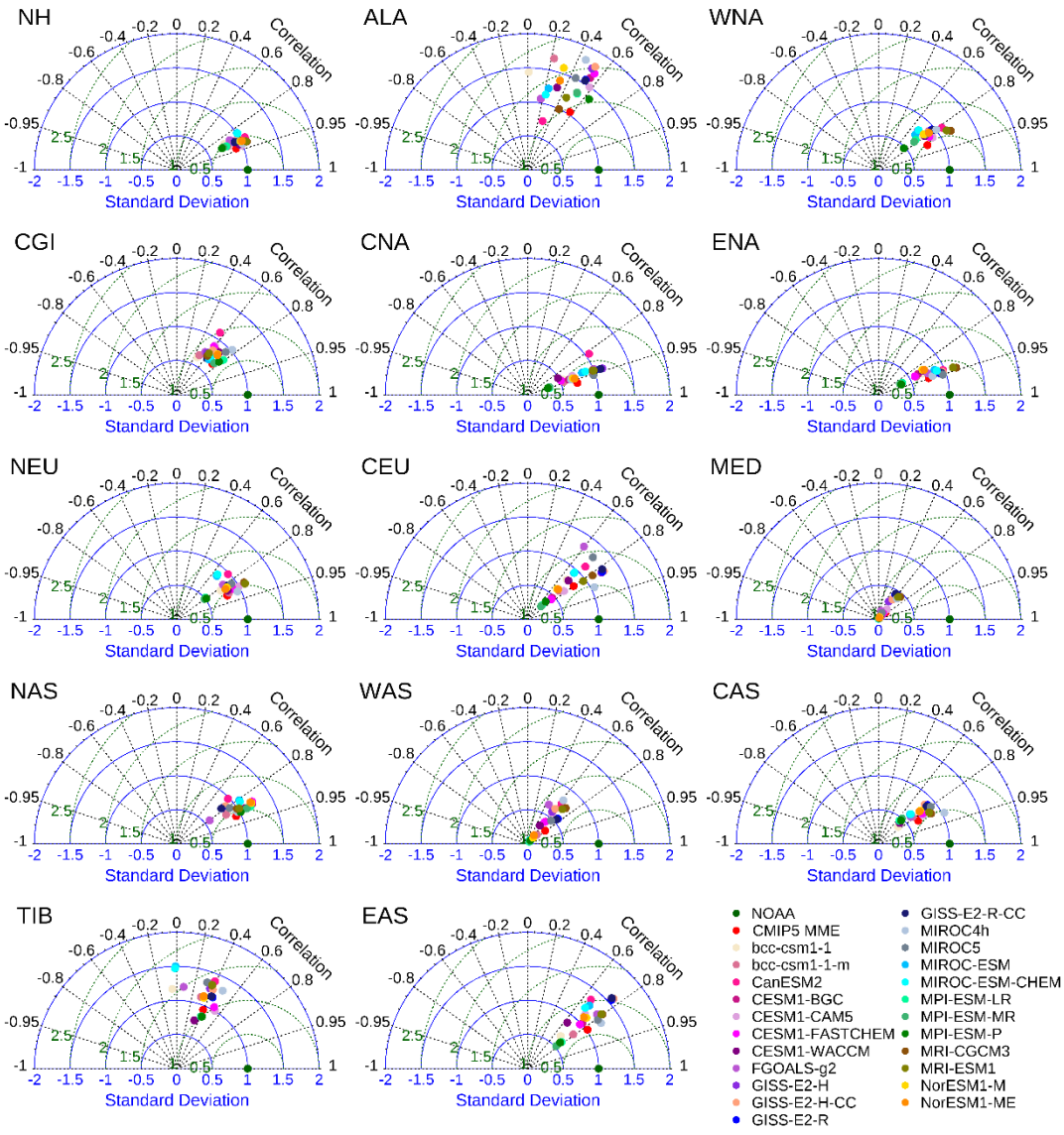

1-NH:Northern Hemisphere
2-ALA:Alaska/N.W Canada
3-WNA:West North America
4-CGI:Canada/not include Greenland/iceland
5-CNA:Central North America
6-ENA:East North America
7-NEU:North Europe
8-CEU:Central Europe
9-MED:South Europe/Mediterranean
10-NAS:North Asia
11-WAS:West Asia
12-CAS:Central Asia
13-TIB:Tibetan Plateau
14-EAS:East Asia

Figure 3. Taylor diagrams of the annual mean spring (March, April and May) SCF in CMIP5 from 1982 to 2005 over the NH and its 13 sub-regions, which are defined in the Fifth Assessment Report (AR5) of the International Panel on Climate Change (IPCC) (IPCC, 2013). Distances from the origin (radius) indicate normalized standard deviations; radial lines (angles) indicate r values; and distances from the reference point indicate RMSEs.

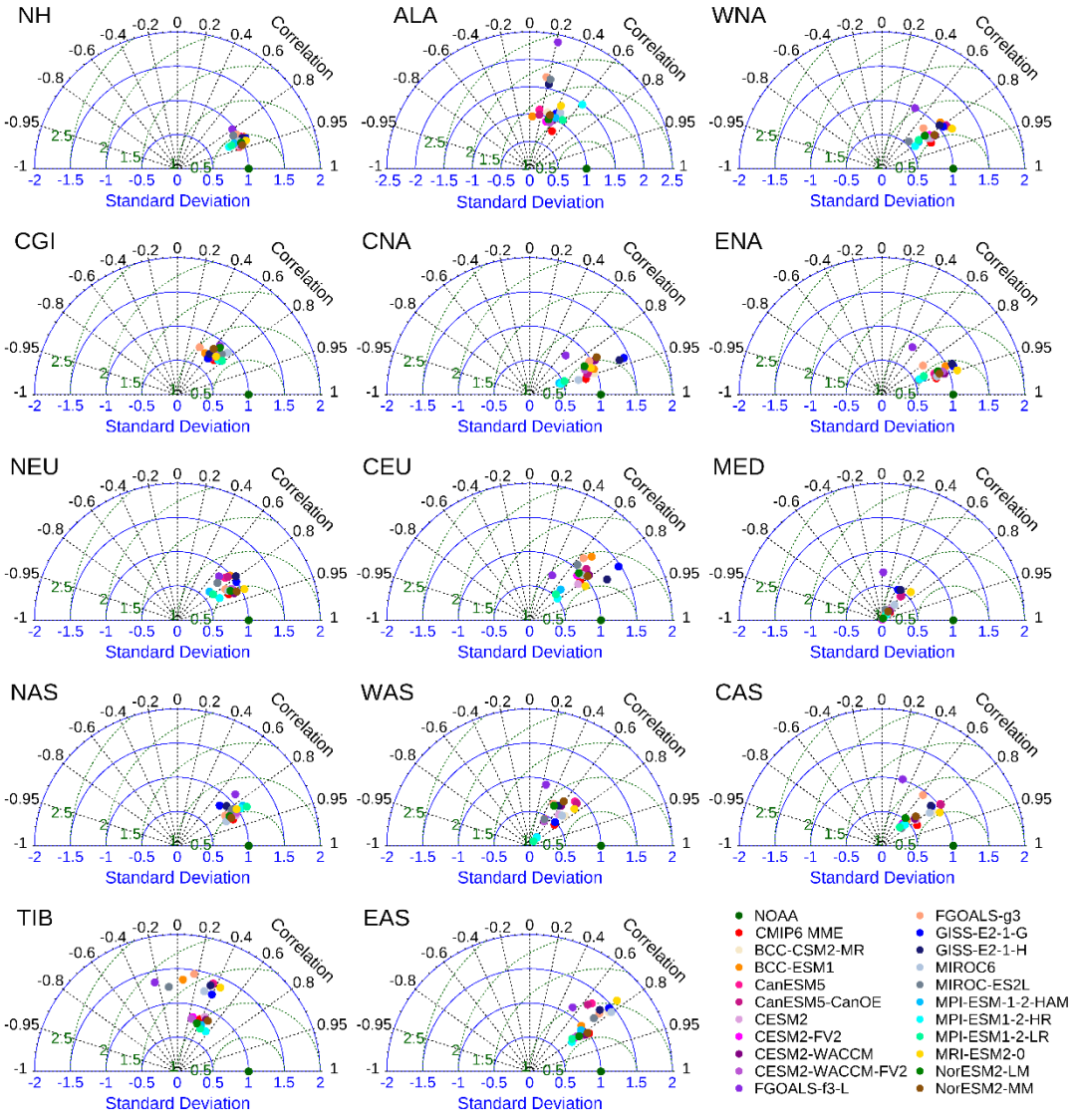

Figure 4. Taylor diagrams of the annual mean spring (March, April and May) SCF in CMIP6 from 1982 to 2005 over the NH and its 13 sub-regions, which

are defined in the IPCC Fifth Assessment Report (AR5) (IPCC, 2013). Distances from the origin (radius) indicate normalized standard deviations; radial lines (angles) indicate r values; and distances from the reference point indicate RMSEs.

3.1.2 Long-term trend evaluation for spring SCF over the NH from 1982 to 2005

Figure5 and Figure 6 illustrate the spatial pattern of long-term spring SCF trends based on the CMIP5 and CMIP6 model simulations and the NOAA data. The NOAA data exhibit a decreasing trend of spring SCF in 57.18% of the NH, 8.98% of which, mainly distributed in part of the WNA and the southern edge of NAS regions, shows a significant decreasing trend. In contrast, the spring SCF trend in the eastern TIB region shows a significant increasing trend of greater than 10%/10 yr. Most model simulations from CMIP5 and CMIP6 can capture the decreasing trend in parts of the WNA and the southern edge of the NAS as the NOAA dataset does. However, over the TIB, only a few model simulations (CMIP5: bcc-csm1-1-m, CESM1-FASTCHEM, CESM1-WACCM, GISS-E2-H, MIROC-ESM, MIROC5, MRI-CGCM3, and MRI-ESM1; CMIP6: MIROC6 and MRI-ESM2-0) can capture the increasing trend that is consistent with NOAA data. For MME, the CMIP5 and CMIP6 MMEs fail to capture the increasing trend of spring SCF in the eastern part of the TIB, CNA, ENA, and CEU regions and the western part of the NAS region. Moreover, the CMIP5 and CMIP6 MMEs simulate a decreasing trend of SCF over 89.32% and 93.75% of the NH, respectively, which far exceeds that of the NOAA data (57.18%).

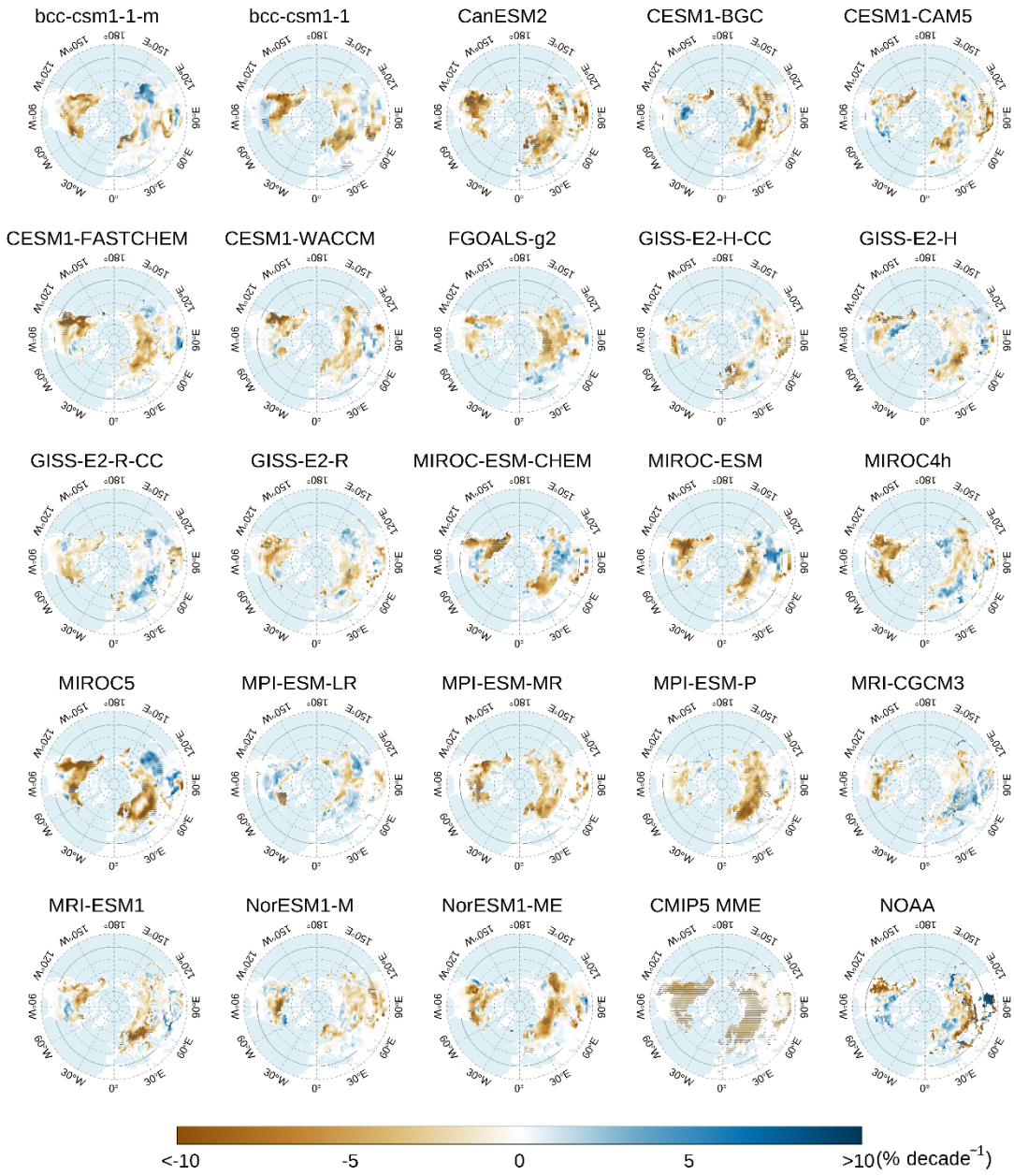

Figure 5. Spatial pattern of the long-term trends in spring SCF of each CMIP5 model simulation as well as the CMIP5 MME and NOAA data during 1982-2005 over the NH. The hatched areas indicate statistically significant trends at the 95% confidence level.

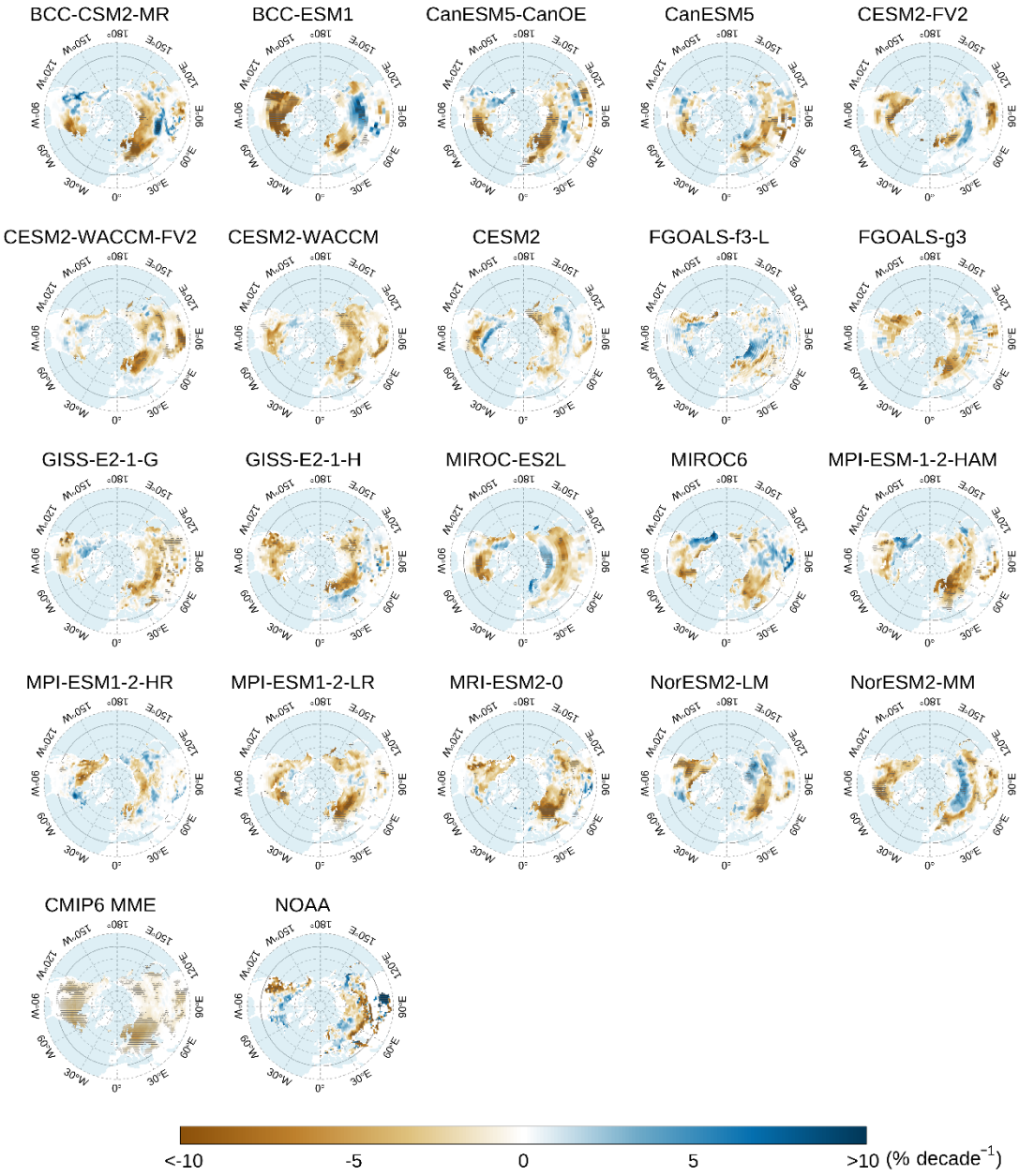

Figure 6. Spatial pattern of the long-term trends in spring SCF of each CMIP6 model simulation as well as the CMIP6 MME and NOAA data during 1982-2005 over the NH. The hatched areas indicate statistically significant trends at the 95% confidence level.

The relative bias (Figure 7, Figure 8) is further used to quantitatively assess the

ability of each model simulation to simulate long-term spring SCF trends. For the NH, all model simulations in CMIP5 and CMIP6 overestimate the spring SCF reduction trend, with RB values ranging from 0.62-4.14 and 0.93-5.35, respectively. However, the ability to simulate the spring SCF trend of the CMIP6 MME is better than that of the CMIP5 MME (RB values of 0.81 and 0.73 for the CMIP5 MME and CMIP6 MME, respectively). We then evaluate the ability of each model simulation to simulate the spring SCF trends in the 13 sub-regions. For the ALA, CGI, NAS, WAS, CAS, and TIB regions, there is no significant difference among CMIP5 and CMIP6 model simulations, with RB values ranging from -0.98 to 6.77 and -0.97 to 7.26, respectively. However, in the WNA and MED regions, the RB values of MIROC6 in CMIP6 are 7.88 and 3.73, respectively, which are much larger than the RB values of all CMIP5 model simulations (-0.44-3.06 and -0.97-0.41 in WNA and MED, respectively). It should be noted that most model simulations in CMIP5 and CMIP6 perform extremely poorly, with RB values even greater than 20 in the CEU and EAS regions. According to the MME, the RB values are closer to 0 with the CMIP6 MME than with the CMIP5 MME in the WNA, CGI, MED, NAS, WAS, and CAS regions (RB for CMIP5 MME: 0.36, -0.32, -0.82, 0.87, -0.9, and -0.84; RB for CMIP6 MME: -0.14, -0.11, -0.42, 0.2, -0.78, and -0.76, respectively).

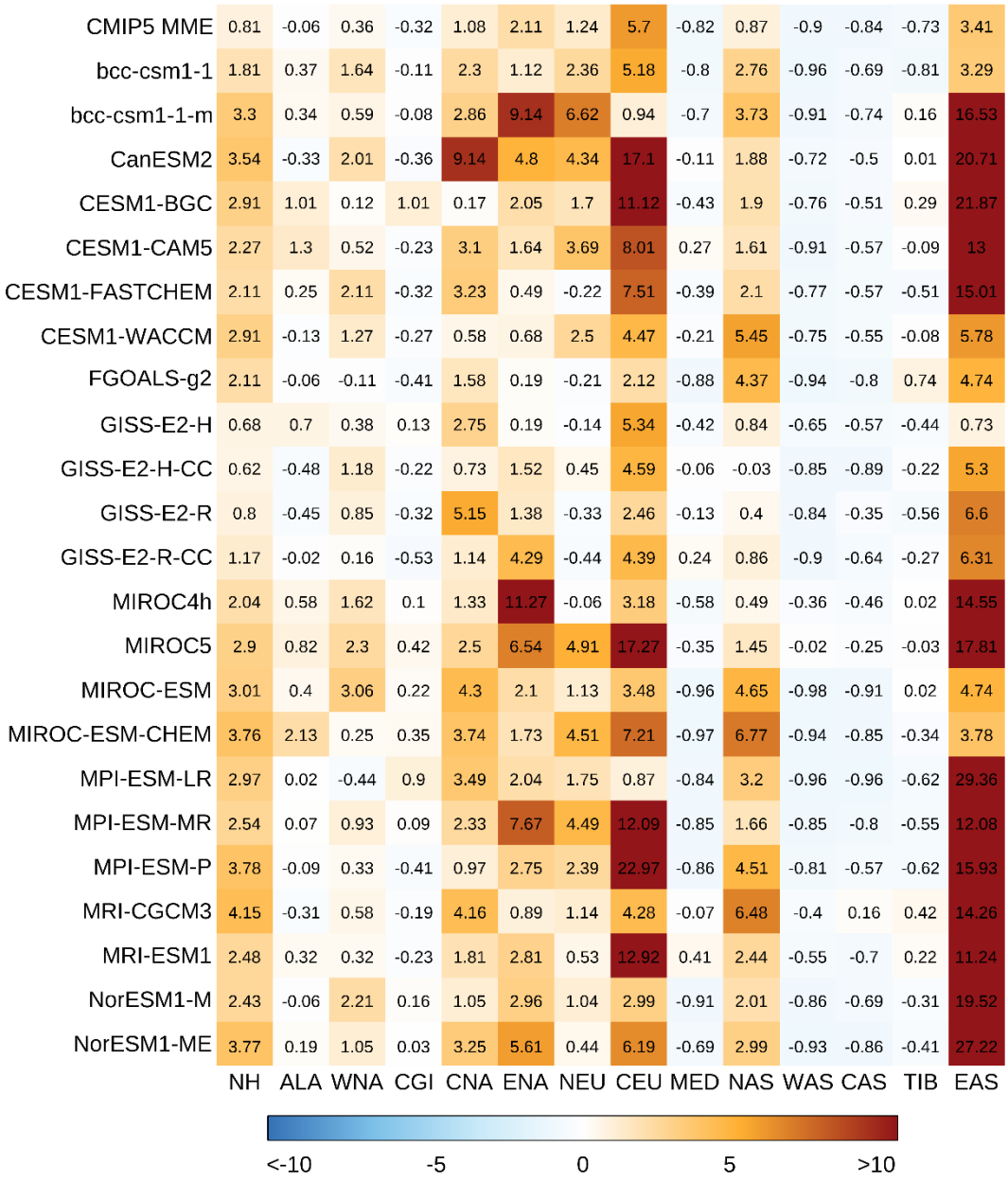

Figure 7. Comparison of the RB of the long-term trend of spring SCF for each CMIP5 model simulation and the CMIP5 MME over 13 sub-regions across the NH during the period of 1982-2005.

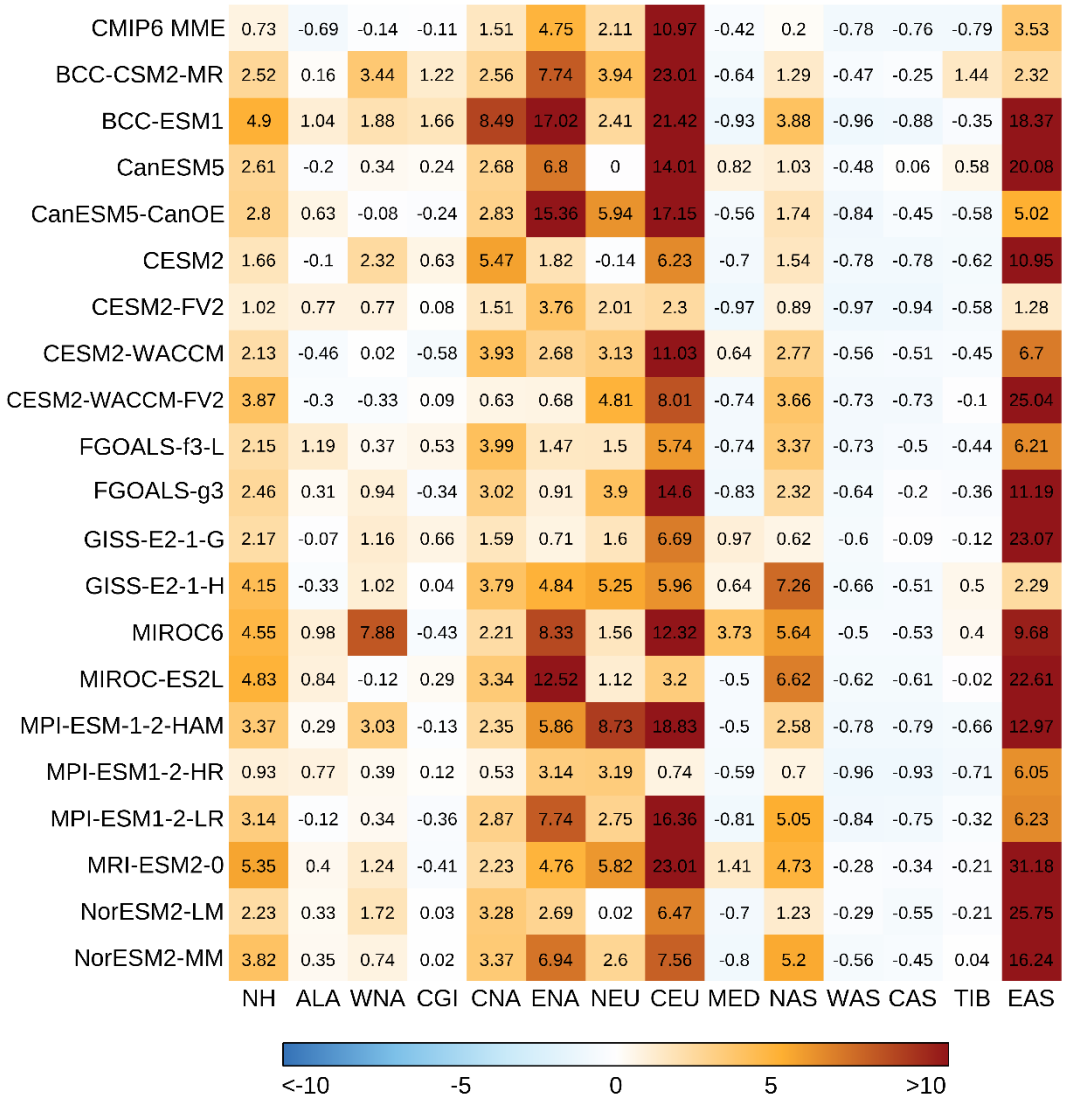

Figure 8. Comparison of the RB of the long-term trend of spring SCF for each CMIP6 model simulation and the CMIP6 MME over 13 sub-regions across the NH during the period of 1982-2005.

3.1.3 Intra-annual variability of spring SCF over the NH from 1982 to 2005

The intra-annual variability in the spring SCF is analysed in Figure 9 and Figure 10. We find a sharp decrease in the spring SCF from March (57.44%) to May (22.44%) over the NH from the NOAA data. All CMIP5 and CMIP6 model

simulations can capture the same characteristics as the NOAA data during the spring season. We find that the simulated SCFs in March (51.38±9.66%), April (38.36±10.21%) and May (21.09±11.51%) from the CMIP6 model simulations and the CMIP6 MME (March, April and May are 53.62%, 40.18% and 20.59, respectively) are closer to the NOAA data than are the CMIP5 (48.30±9.42%, 35.20±12.11% and 17.43±10.82%) and CMIP5 MME (March, April and May are 51.24%, 38.15% and 18.98, respectively). A large variability across models is found in the CMIP5 and CMIP6 simulations of the intra-annual variability of spring SCF for the 13 sub-regions. In contrast, the MME of spring SCF in the CMIP5 and CMIP6 performs better than that of individual models from March to May, although it is slightly overestimated in the TIB and EAS regions. Compared to the CMIP5 MME, CMIP6 MME simulated SCF from March-May over the 13 sub-regions is closer to that of the NOAA data. For example, for the CNA region, the simulated SCFs from March to May are 21.76%, 5.80%, and 0.27%, respectively, and the CMIP6 MME is closer to that of the NOAA data (22.03%, 6.23%, and 0.27%, respectively) than is the CMIP5 MME (18.37%, 4.81%, and 0.19%, respectively).

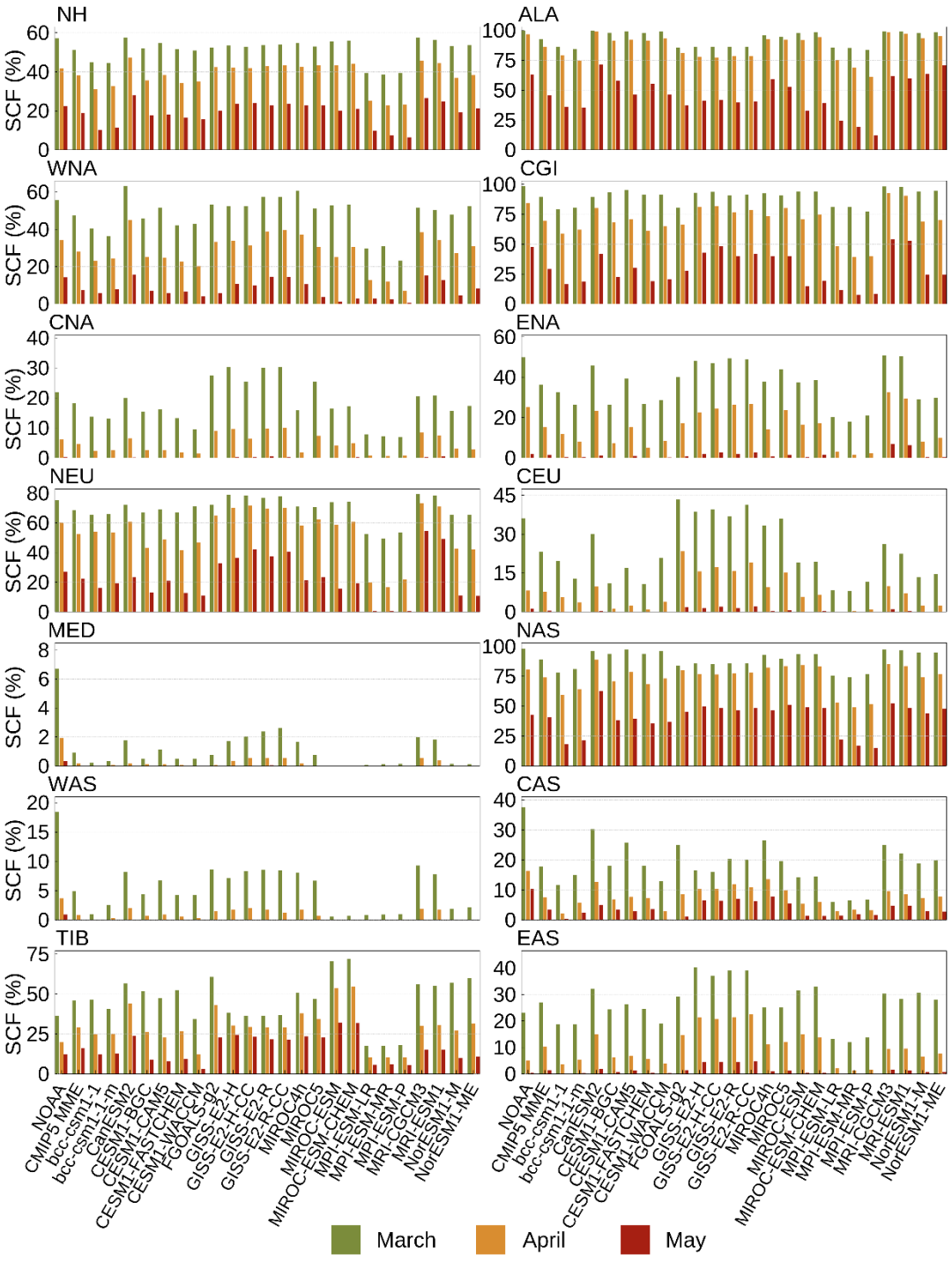
NH
ALA
WNA
CGI
CNA
ENA
NEU
CEU
MED
NAS
WAS
CAS
TIB
EAS
SCF (%)
NOAA
CMIP5 MME
bcc-csm1-1
bcc-csm1-1-m
CanESM2
CESM1-BGC
CESM1-CAM5
CESM1-FASTCHEM
CESM1-WACCM
FGOALS-g2
GISS-E2-H
GISS-E2-H-CC
GISS-E2-R
GISS-E2-R-CC
MIROC4h
MIROC5
MIROC-ESM
MIROC-ESM-CHEM
MPI-ESM-LR
MPI-ESM-MR
MPI-ESM-P
MRI-CGCM3
MRI-ESM1
NorESM1-M
NorESM1-ME
March
April
May

Figure 9. Mean monthly (March-May) SCF by each CMIP5 model, the CMIP5 MME and the NOAA data during the period of 1982–2005 over the NH and its 13 sub-regions.

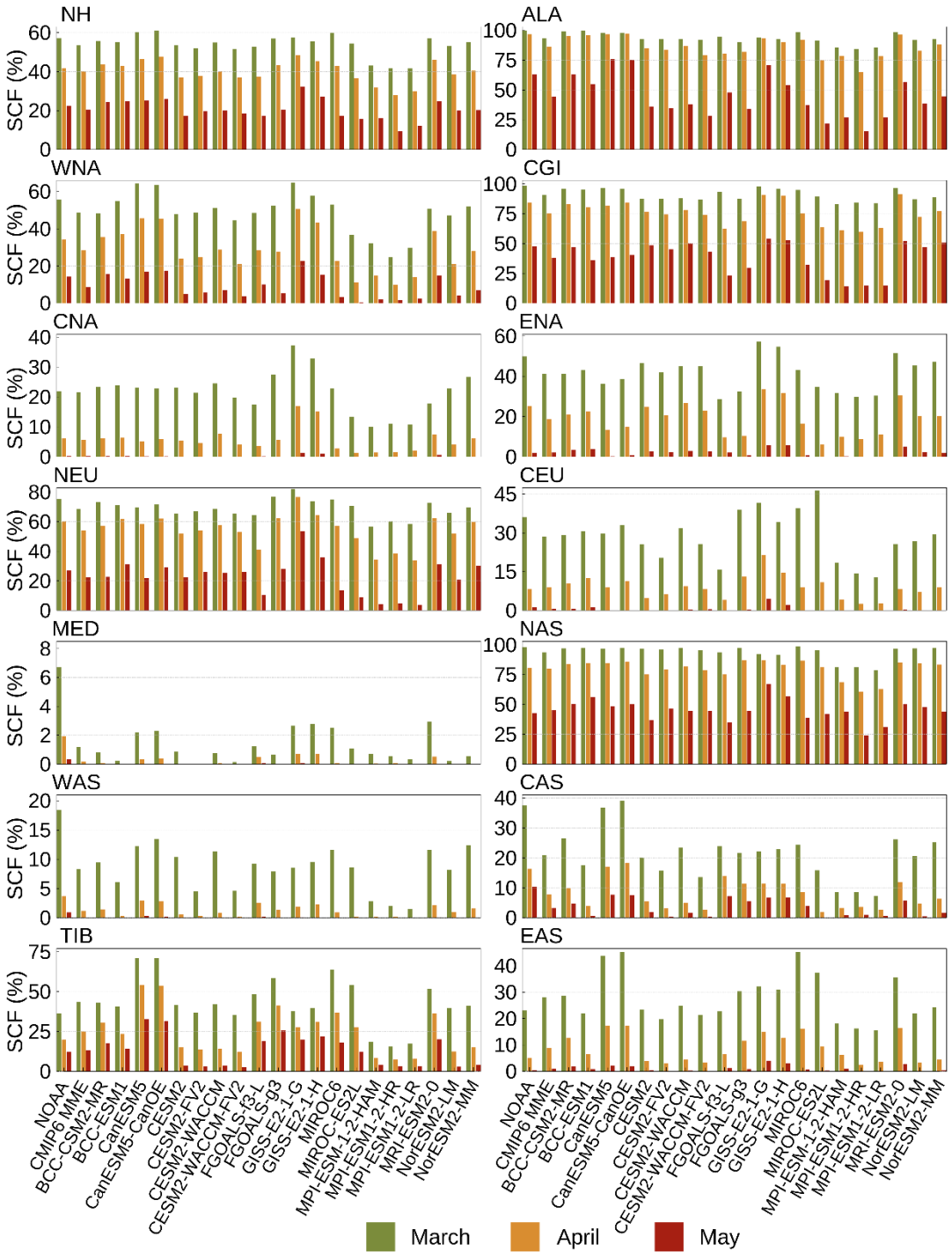
NH
ALA
WNA
CGI
CNA
ENA
NEU
CEU
MED
NAS
WAS
CAS
TIB
EAS
SCF (%)
NOAA
CMIP6 MME
BCC-CSM2-MR
BCC-ESM1
CanESM5
CanESM5-CanOE
CESM2
CESM2-FV2
CESM2-WACCM
CESM2-WACCM-FV2
FGOALS-f3-L
FGOALS-g3
GISS-E2-1-G
GISS-E2-1-H
MIROC6
MIROC-ES2L
MPI-ESM-1-2-HAM
MPI-ESM1-2-HR
MPI-ESM1-2-LR
MRI-ESM2-0
NorESM2-LM
NorESM2-MM
March
April
May

Figure 10. Mean monthly (March-May) SCF by each CMIP6 model, the CMIP6 MME and the NOAA data during the period of 1982–2005 over the NH and its 13 sub-regions.

Then, we use the CRIac values based on the bias, RSME, and r to assess the ability of each model simulation to simulate the intra-annual spring SCF (Figure 11, Figure 12). The results show that the CMIP6 model simulations have slightly larger CRIac values than do the CMIP5 simulations (the range of CRIac values for the CMIP5 and CMIP6 models are 0.12-0.73 and 0.21-0.78, respectively) across the NH. Moreover, only one of the twenty-three CMIP5 models (MIROC4h) has a CRIac value greater than 0.7, while four of the twenty CMIP6 models (BCC-ESM1, CESM2-WACCM, FGOALS-g3, and NorESM2-MM) have a CRIac value greater than 0.7. For the MME, the CRIac value of the CMIP6 MME (0.65) is larger than that of most individual models and is larger than that of the CMIP5 MME (0.45). The above results indicate that the CMIP6 is better than the CMIP5 in simulating the climatological spring SCF over the NH.

The number of models with CRIac values greater than 0.7 is relatively higher in the CMIP6 than in the CMIP5 for most regions. For example, for the CEU, only one of the twenty-three CMIP5 models (MIROC4h) has a CRIac value greater than 0.7, while four of the twenty CMIP6 models (CanESM5, CanESM5-CanOE, CESM2-WACCM, and MIROC6) have a CRIac value greater than 0.7. For MME, the CRIac values for the CMIP5 MME and CMIP6 MME are larger than most individual models in the 13 sub-regions, indicating that the MME is better than the individual models in simulating the intra-annual variability of spring SCF. Comparing the CMIP5 MME and CMIP6 MME, we find that the CRIac value of the CMIP5 MME (0.49) is greater than that of the CMIP6 MME (0.44) only in the ALA region, while in the remaining 12 regions, the CRIac values of the CMIP5 MME are smaller than those of the CMIP6 MME (e.g., for the CNA region, the CRIac values of the CMIP5 MME and CMIP6 MME are 0.68 and 0.9, respectively), suggesting that the CMIP6 MME is better able to simulate the intra-annual variability of spring SCF in these 12 regions.

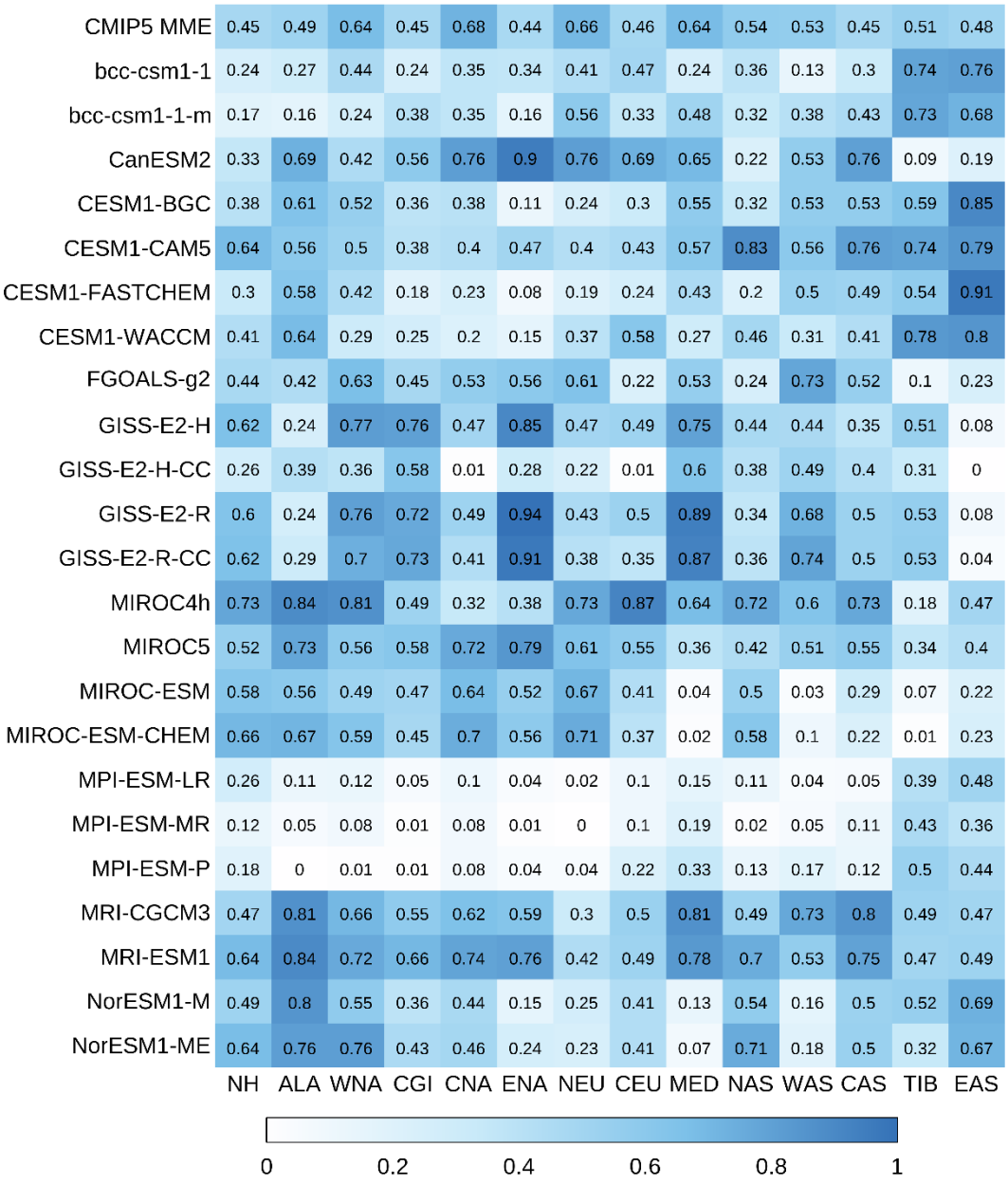

Figure 11. CRIac statistical heatmap of each CMIP5 model and the CMIP5 MME for the NH and its 13 sub-regions.

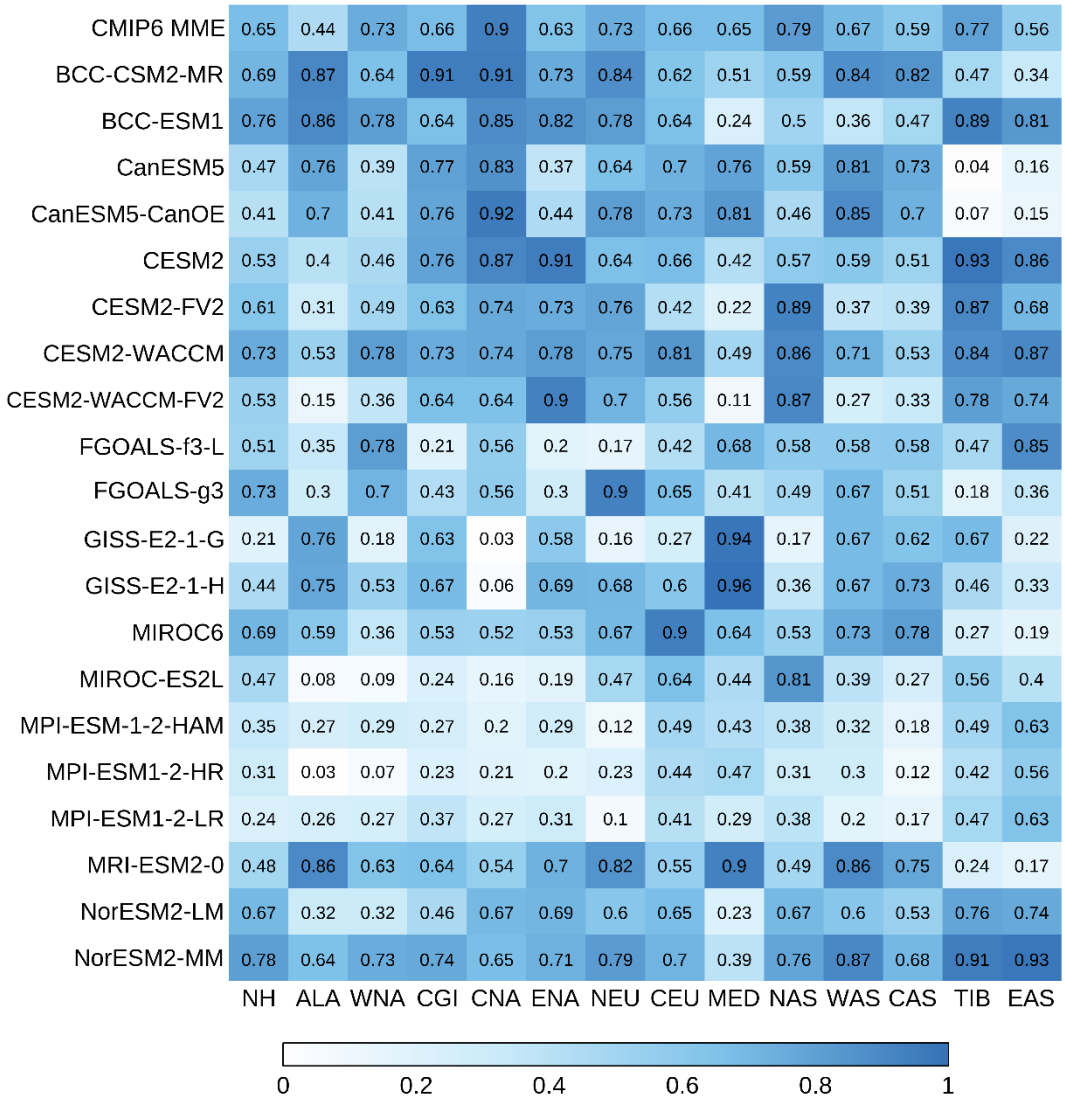

Figure 12. CRIac statistical heatmap of each CMIP6 model and the CMIP6 MME for the NH and its 13 sub-regions.

3.1.4 Assessment of overall model performance

This section focuses on quantitatively assessing the overall model performance in simulating the spring SCF using an integrated method (CRI). The CRI value is calcu-lated by TSS, RB and CRIac for each model simulation, and then an arithmetic mean is calculated through CRI values from different model simulations by the same institution to assess the overall ability of different institutions

to simulate the spring SCF with the two generations of models (Figure 13). For the NH (Figure 13a), 60% of the institutions using CMIP6 (with the exception of NASA-GISS, MIROC and MRI) have higher CRI values than those using CMIP5, with BCC being the most evident (0.24 and 0.6 in CMIP5 and CMIP6, respectively). The CMIP6 MME has a CRI value of 0.89, which is significantly greater than the CMIP5 MME (0.71). In most of the 13 sub-regions, more institutions show a 'better' simulation ability than a 'worse' one in CMIP6, and this is particularly evident in the WAS region, where all nine institutions in this region show a 'better' simulation ability (Figure 13k). However, in the ALA, WNA and ENA regions, the number of institutions with a 'better' simulation ability in CMIP6 is smaller than the number of institutions with a 'worse' one. Additionally, we find that the MME is significantly better for most individual institutions in CMIP5 and CMIP6, but the CRI values for the CMIP6 MME are greater than those for the CMIP5 MME, except for in the ALA and NEU regions.

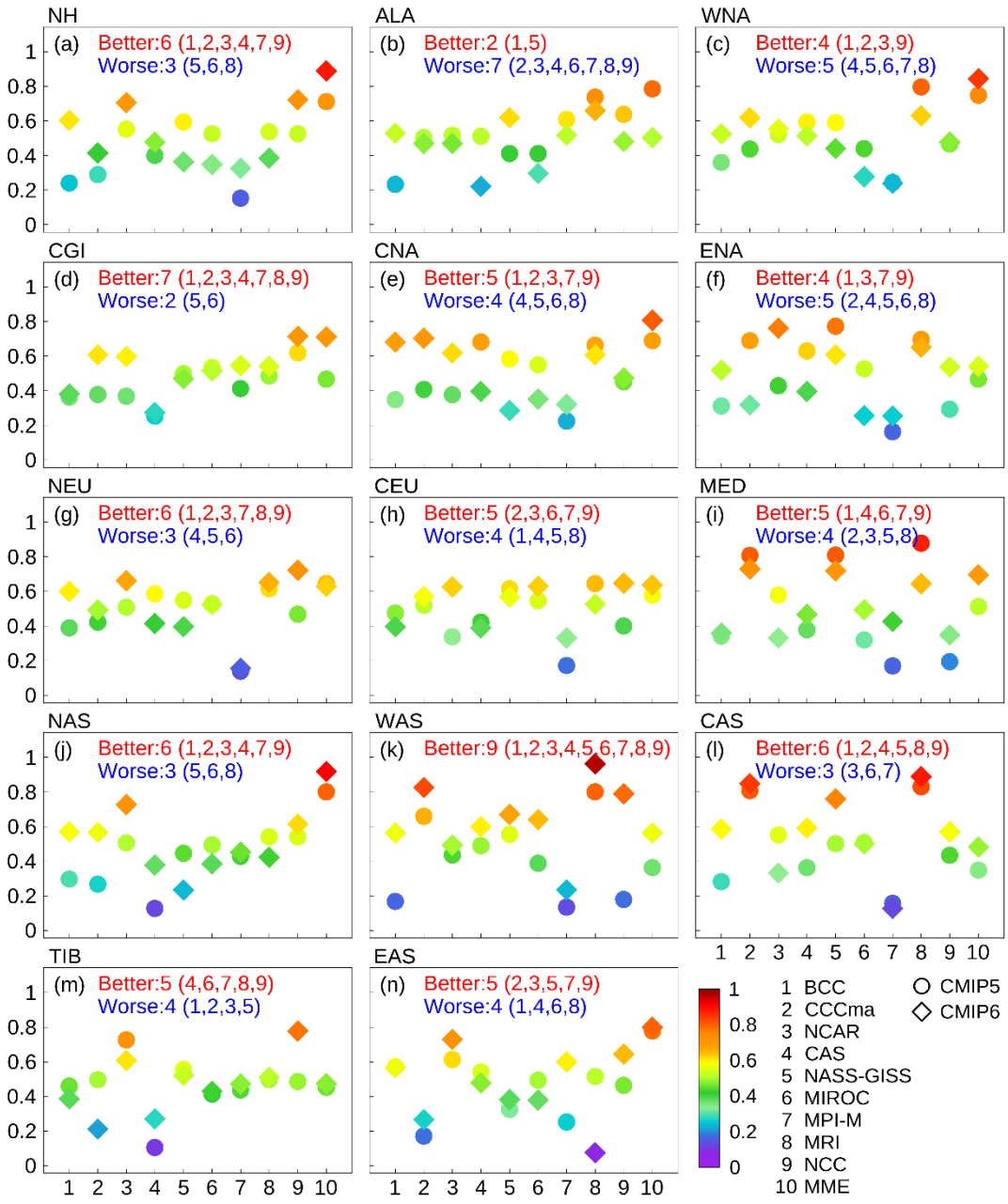

Figure 13. Statistical CRI diagram for CMIP5 and CMIP6 simulations of different institutions as well as the MME across the NH and its 13 sub-regions. The arithmetic mean of the CRI values of the models from the same institution is used as the CRI value of the institution. Circles indicate CMIP5 and diamonds

indicate CMIP6 values. The closer the CRI value is to 1, the stronger the comprehensive simulation ability of the model; red font indicates that the comprehensive simulation ability of the institution in the CMIP6 becomes stronger, and the blue font indicates that the comprehensive simulation ability of the institution in the CMIP6 becomes worse.

3.2 Predicted characteristics of SCF changes in future projections

3.2.1 Spatial pattern variability of the annual mean spring SCF from 2072 to 2095

Figure 14 presents the spatial pattern variability of the annual mean spring SCF for the CMIP5 and CMIP6 under three scenarios during the period of 2072-2095 compared to the baseline of 1982-2005. The projected spring SCF simulated by the CMIP5 MME and CMIP6 MME under different scenarios exhibits a widespread reduction over the NH, especially at the western edge of the NAS. The reduction in SCF becomes increasingly significant with increasing emission concentrations. For example, the spring SCF simulated by the CMIP5 MME and CMIP6 MME shows a slight reduction from -24% to 0% in most regions under the low emissions scenarios (RCP 2.6 and SSP1-2.6) and an obvious reduction in spring SCF from -50% to 0% in the CMIP5 MME and CMIP6 MME following the high emissions scenarios (RCP 8.5 and SSP5-8.5). Compared to that in the RCP 2.6 scenario (95.17%), the spring SCF reduction area (92.62%) is decreased under the SSP1-2.6 scenario. The same results are shown under the medium emissions scenarios (RCP 4.5: 95.26%; SSP2-4.5: 94.80%). In contrast, compared to that in the RCP 8.5 scenario (92.74%), the spring SCF reduction area (97.55%) is expanded under the SSP5-8.5 scenario.

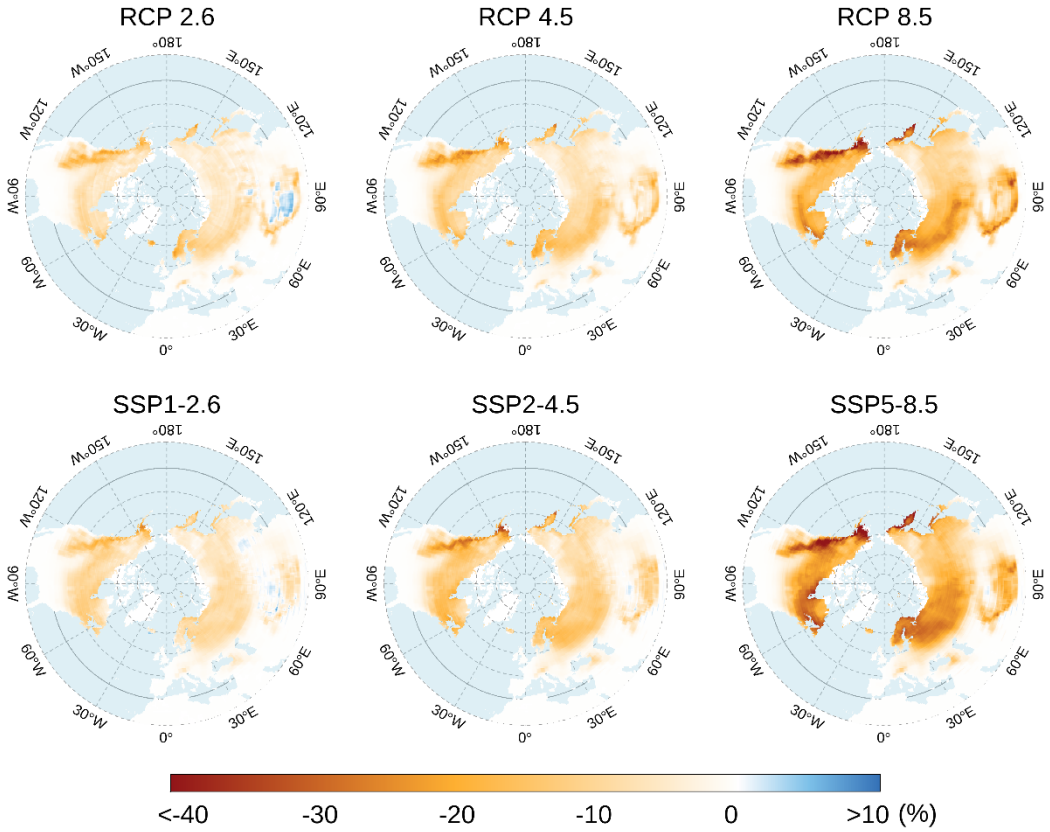

Figure 14. Spatial pattern of spring SCF changes in the CMIP5 and CMIP6 under different scenarios for the future period (2072-2095) compared to the historical period (1982-2005).

3.2.2 Interannual variability in spring SCF over the NH from 2006 to 2099

Based on the interannual variability in spring SCF from 1982-2099 (Figure 15, Figure 16), the spring SCF exhibits a fluctuating decrease across the NH and its 13 sub-regions under all RCP and SSP scenarios. Specifically, the spring SCF under different scenarios (RCPs or SSPs) shows relatively consistent changes until 2040, while the changes significantly differ after 2040. Additionally, the long-term trends under the RCP 2.6 and SSP1-2.6 scenarios are very similar at -0.26%/10 yr and -0.27%/10 yr, respectively, and the larger SCF reduction trends under the RCP 4.5 and SSP2-4.5 scenarios have trends of -0.59%/10 yr and -0.68%/10 yr, respectively. The strongest SCF reduction trends are found under the RCP 8.5 and SSP5-8.5 scenarios, with trends of -1.26%/10 yr and -1.59%/10 yr, respectively. Similar to those of the whole NH, the future trends in spring SCF vary significantly among the sub-regions from 2040 onwards under

different emission scenarios. The significant decreasing trends of spring SCF are mainly found in the ALA, WNA, CGI, ENA, NEU, NAS, and TIB regions, with approximately -0.23%/10 yr under the RCP 2.6 and SSP1-2.6 scenarios, -0.57%/10 yr under the RCP 4.5 and SSP2-4.5 scenarios, and -1.23%/10 yr under the RCP 8.5 and SSP5-8.5 scenarios. It is worth noting that there is an extremely low decreasing trend in the MED region under the three scenarios, which is due to the extremely low SCF in that region, where the annual mean SCF is less than 1% (Figure S1 and Figure S2 in Supporting Information S1). By comparing the spring SCF changes simulated by the CMIP5 MME and CMIP6 MME under the same emissions scenarios, we find that the decreasing trend of spring SCF in the SSPs is much larger than that in the RCPs, except for the CGI and NEU regions under the SSP1-2.6 and RCP 2.6 scenarios and the NEU region under the SSP2-4.5 and RCP 4.5 scenarios.

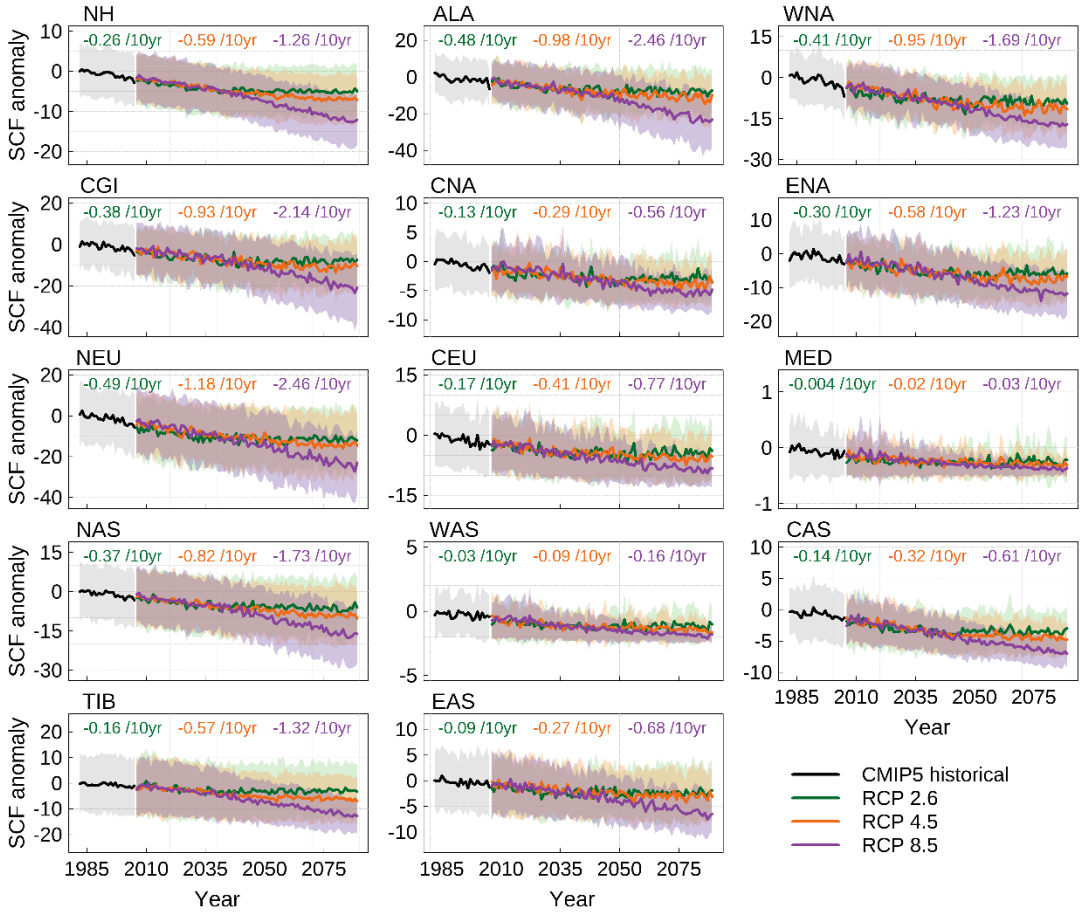

Figure 15. Time series plots of spring SCF anomalies in the NH and its 13 sub-regions from 1982-2099. Different colours indicate the SCF anomaly values under different scenarios in the CMIP5; shaded areas indicate one standard

deviation range under different scenarios.

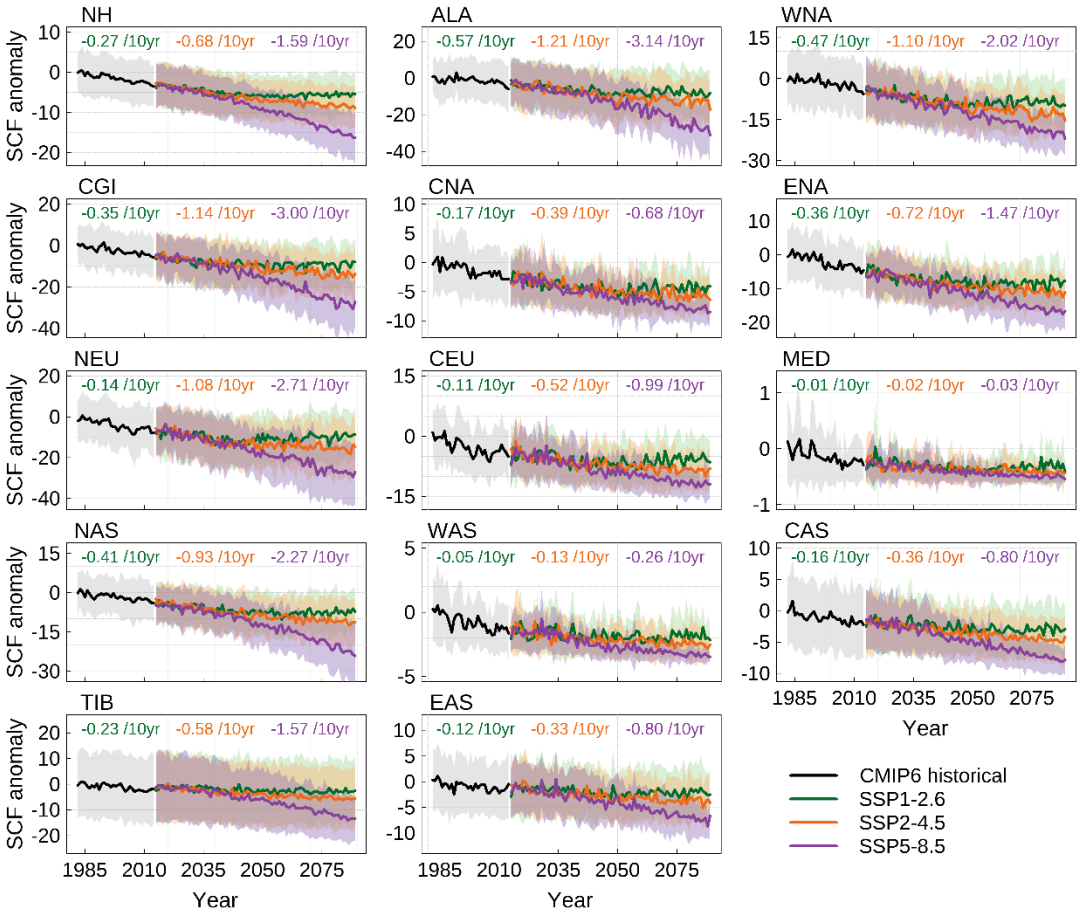

Figure 16. Time series plots of spring SCF anomalies in the NH and its 13 sub-regions from 1982-2099. Different colours indicate the SCF anomaly values under different scenarios in the CMIP6; shaded areas indicate one standard deviation range under different scenarios.

4 Discussion

Snow is an indispensable component of the cryosphere and has an important im-pact on the energy balance of the Earth's climate system. It has been widely considered one of the most important mechanisms for warming (i.e., Arctic amplification, Pithan & Mauritsen, 2014) and an important factor in assessing changes in the amount of water resources at global and/or regional scales (e.g., Milly & Dunne, 2020; Lutz et al., 2022). Models are powerful tools for understanding and forecasting the spring SCF changes that are influenced by climate change across the NH. By analysing the annual mean, long-term trend and intra-annual variability of the spring SCF against NOAA data, we find that

there is not a single model in the CMIP5 nor the CMIP6 that could satisfactorily capture the spatial and temporal characteristics of the NOAA data across the globe and in the 13 sub-regions of the NH.

However, the majority of the institutions using CMIP6 have higher CRI values than those using CMIP5 across the NH, and the number of institutions with a 'better' simulation ability in CMIP6 is greater than the number of institutions with a 'worse' simulation ability in most regions according to the comprehensive assessment.

We emphasize that the improvements in the new state-of-the-art CMIP6 model simulations can be attributed to three major sources: meteorological forcing data, model structure and parameterizations and spatial resolution (e.g., Decharme, 2007; Jin et al., 2021; van Kempen et al., 2021; Li et al., 2021). Meteorological forcing data, especially precipitation and temperature, strongly affect CMIP simulations through the snow generation process, as precipitation and temperature are the primary and direct sources that control the amount of snow (e.g., Mankin & Diffenbaugh, 2015; Tang et al., 2017). For example, the severe overestimation of the annual mean spring SCF over the TIB and EAS regions (Figure 1) in CMIP5 is strongly related to the cold bias (Figure S3 in Supporting Information S1) and overestimation of precipitation (Figure S5 in Supporting Information S1); however, the large bi-as in temperature and precipitation has been improved in CMIP6 (Figure S4 and Figure S6 in Supporting Information S1). In other regions (except WAS and NAS), the underestimation of the annual mean spring SCF in CMIP6 improves relative to the results of the CMIP5, mainly re-lated to the corrected overestimation of temperature (Figure S3 and Figure S4 in Supporting Information S1). The relationship between temperature and SCF in spring is observed in CMIP5 and CMIP6 models (Brutel-Vuilmet et al., 2013; Mudryk et al., 2017) indicating that ESMs should further improve temperature simulations. Previous studies have shown that cli-mate models have had difficulties correctly reproducing seasonal snow (Brutel-Vuilmet et al., 2013; Derksen & Brown, 2012; Henderson et al., 2018; Santolaria-Otín & Zolina, 2020; Thackeray et al., 2016). However, the present study shows that a low bias of intra-annual variability in the spring season in CMIP5 is largely corrected in the CMIP6 (Figure 9, Figure 10), which is consistent with Zhu et al. (2021), Mudryk et al. (2020) and Kouki et al. (2021). The lower snowmelt rate based on low temperature bias from the new model parameterizations and structures in CMIP6 (Kouki et al., 2021; Mudryk et al., 2020) during the snow melting season (Figure S3 and Figure S4 in Supporting Information S1) could partly explain this correction. In addition, model simulation ability is also related to spatial resolution (Wu et al., 2021). For example, the spatial resolution of the models of the BCC, CAS, MPI-M and NCC institutions is improved in CMIP6 compared to that in CMIP5 (Table S1 in Supporting Information S1); therefore, for these four institutions, the overall model performance in simulating spring SCF over the NH is better in CMIP6 than in CMIP5 (Figure 13a).

The multi-model ensemble mean is often reported to outperform individual models (e.g., Ahmed et al., 2019; Gudmundsson, 2011; Guo et al., 2021; Santolaria-Otín & Zolina, 2020). Our analysis shows that simple averages generally outperform most individual models for all metrics. However, the deteriorated performance of simple averages in capturing all three aspects of our study in some areas suggests that the simple ensemble mean method may not be suitable for assessing some specific regions. This suggests that more sophisticated multi-model ensemble methods, such as Bayesian averages (Raftery et al., 2005) or weighting averages (Kulinich et al., 2021), may prove to be more helpful than simple averages.

5 Conclusions

In this study, we use NOAA data as reference data to evaluate the spring SCF simulation ability of each model simulation from CMIP5 and CMIP6 and their MMEs as well as future changes in RCPs and SSPs across the NH and its 13 sub-regions.

(1) Compared to the NOAA data, the spring SCF that was simulated by CMIP5 and CMIP6 models and their MMEs show generally negative biases over most of the NH regions and generally positive biases over the TIB and EAS regions during the period of 1982-2005. And most of the model simulations can capture the decreasing trends in parts of the WNA and the southern edge of the NAS region, however, only a few model simulations can present the increasing trend over the TIB region. In addition, most model simulations generate a lower monthly climatological SCF (March-May) in most regions and a higher monthly climatological SCF in the TIB region across the NH.

(2) The models have differences in performance for simulating different aspects of spring SCF. However, MMEs perform better compared to most of the model simulations. In terms of the comprehensive assessment, the majority of the institutions using CMIP6 had higher CRI values than those using CMIP5 across the NH. The number of institutions with a 'better' simulation ability using CMIP6 is greater than the number of institutions with a 'worse' simulation ability in most regions, and vice versa in the ALA, WNA and ENA regions. It is important to note that the CRI values for the CMIP6 MME are greater than those for the CMIP5 MME, except for the ALA and NEU regions, suggesting that the overall performance of the CMIP6 MME in simulating the spring SCF improves in other 11 regions.

(3) Projections indicate future reductions in spring SCF over the NH during the period of 2072-2095, particularly over the ALA, WNA and NEU regions. Meanwhile, the spring SCF has a reduced rate with increasing emissions, with lower rates in scenarios with lower emissions. The predicted spring SCF trend by the CMIP5 MME and CMIP6 MME over the NH and its 13 sub-regions shows a decreasing trend from 2006 to 2099; while there is no significant difference between the CMIP5 and CMIP6 scenarios until 2040, they rapidly diverge thereafter. For the same emissions scenario, the CMIP6 MME simulates a stronger reduction

trend in SCF in the NH than does the CMIP5 MME.

Acknowledgments

We are grateful for the support of the National Natural Science Foundation of China (Nos. 41861014 and 42101030), Natural Science Foundation of Inner Mongolia (Nos. 2022MS04004, 2020BS03042 and 2020BS04009), Open Project of the Remote Sensing and Geographic Information System Application Laboratory with the State Key Laboratory of the Xinjiang Uygur Autonomous Region (No. XJYS0205-201901), Key Research and Development (R&D) and Achievement Transformation Project of the Inner Mongolia Autonomous Region (No. 2022YFDZ0061), and Talent Project of Science and Technology in Inner Mongolia (No. NJYT22027).

Open Research

Data Availability Statement

The NH EASE Grid 2.0 Weekly Snow Cover and Sea Ice Extent dataset from the NOAA/NCDC are available at https://data.nodc.noaa.gov; Monthly temperature and precipitation data from CRU TS, 4.04, are available at https://crudata.uea.ac.uk/cru/data/hrg/; CMIP5 and CMIP6 model outputs are available at https://esgf-node.llnl.gov/search/cmip5/ and https://esgf-node.llnl.gov/search/cmip6/ respectively.

References

Ahmed, K., Sachindra, D. A., Shahid, S., Demirel, M. C., & Chung, E. -S. (2019). Selection of multi-model ensemble of general circulation models for the simulation of precipitation and maximum and minimum temperature based on spatial assessment metrics. *Hydrology and Earth System Sciences*, **23**(11), 4803–4824. https://doi.org/10.5194/hess-23-4803-2019

Barnett, T. P., Adam, J. C., & Lettenmaier, D. P. (2005). Potential impacts of a warming climate on water availability in snow-dominated regions. *Nature*, **438**(7066), 303-309. https://doi.org/doi:10.1038/nature04141

Barnhart, T. B., Molotch, N. P., Livneh, B., Harpold, A. A., Knowles, J. F., & Schneider, D. (2016). Snowmelt rate dictates streamflow. *Geophysical Research Letters,* **43**(15), 8006-8016. https://doi.org/10.1002/2016GL069690

Bellprat, O., Guemas, V., Doblas-Reyes, F., & Donat, M. G. (2019). Towards reliable extreme weather and climate event attribution. *Nature communications,* **10**, 1732. https://doi.org/10.1038/s41467-019-09729-2

Bormann, K. J., Brown, R.,D., Derksen, C., & Painter, T.,H. (2018). Estimating snow-cover trends from space. *Nature Climate Change,* **8**(11), 924-928. https://doi.org/10.1038/s41558-018-0318-3

Brodzik, M. J., & Armstrong, R. (2013). Northern Hemisphere EASE-Grid 2.0 Weekly Snow Cover and Sea Ice Extent, Version 4. [Indicate subset used]. Boulder, Colorado USA. NASA National Snow and Ice Data Center Distributed Active Archive Center. 2013. https://doi.org/10.5067/P7O0HGJLYUQU [Date Accessed]

Brown, R. D., Derksen, C., & Wang, L. B. N. (2010). A multi-data set analysis of variability and change in Arctic spring snow cover extent. *Journal of Geophysical Research: Atmospheres*, **115**, D16111. https://doi.org/10.1029/2010JD013975

Brown, R. D., & Robinson, D. A. (2011). Northern Hemisphere spring snow cover variability and change over 1922-2010 including an assessment of uncertainty. *The Cryosphere*, **5**(1), 219-229. https://doi.org/10.5194/tc-5-219-2011

Brown, R. D., Schuler, D. V., Bulygina, O., Derksen, C., Luojus, K., Mudryk, L., Wang, L., & Yang, D. (2017). Arctic terrestrial snow cover. In: Snow, Water, Ice and Permafrost in the Arctic (SWIPA). Arctic Monitoring and Assessment Programme (AMAP), Oslo, Norway. pp. 25-64.

Brutel-Vuilmet, C., Ménégoz, M., & Krinner, G. (2013). An analysis of present and future seasonal Northern Hemisphere land snow cover simulated by CMIP5 coupled climate models. *The Cryosphere,* **7**(1), 67-80, https://doi.org/10.5194/tc-7-67-2013

Chen, F., Xu, Q., Chen, J., Birks, H. J. B., Liu, J., Zhang, S., Jin, L., et al. (2015). East Asian summer monsoon precipitation variability since the last deglaciation. *scientific Reports,* **5**(1), 11186. https://doi.org/10.1038/srep11186

Coll, J., & Li, X. G. (2018). Comprehensive accuracy assessment of modis daily snow cover products and gap filling methods. *ISPRS Journal of Photogrammetry and Remote Sensing,* **144**(38), 435–452. https://doi.org/10.1016/j.isprsjprs.2018.08.004

Decharme, B. (2007). Influence of runoff parameterization on continental hydrology: Comparison between the Noah and the ISBA land surface models. *Journal of Geophysical Research: Atmospheres,* **112**(D19). https://doi.org/10.1029/2007JD008463

Derksen, C., & Brown, R. (2012). Spring snow cover extent reductions in the 2008-2012 period exceeding climate model projections. *Geophysical Research Letters,* **39**(19), L19504. https://doi.org/10.1029/2012GL053387

Déry, S. J., & Brown, R. D. (2007). Recent Northern Hemisphere snow cover extent trends and implications for the snow-albedo feedback. *Geophysical Research Letters,* **34**(22), L22504. https://doi.org/10.1029/2007GL031474

Euskirchen, E. S., McGuire, A. D., & Chapin, F. S. (2007). Energy feedbacks of northern high-latitude ecosystems to the climate system due to reduced snow cover during 20th century warming. *Global Change Biology,* **13**(11), 2425-2438. https://doi.org/10.1111/j.1365-2486.2007.01450.x

Eyring, V., Bony, S., Meehl, G. A., Senior, C. A., Stevens, B., Stouffer, R. J., & Taylor, K. E. (2016). Overview of the coupled model intercomparison project phase 6 (CMIP6) experimental design and organization. *Geoscientific Model Development,* **9**(5), 1937-1958. https://doi.org/10.5194/gmd-9-1937-2016

Fernandes, R., Zhao, H., Wang, X., Key, J., Xin, Q., & Hall, A. (2009). Controls on Northern Hemisphere snow albedo feedback quantified using satellite Earth observations. *Geophysical Research Letters,* **36**(21), L21702. https://doi.org/10.1029/2009GL040057

Flanner, M. G., Shell, K. M., Barlage, M., Perovich, D. K., & Tschudi, M. A. (2011). Radiative forcing and albedo feedback from the Northern Hemisphere cryosphere between 1979 and 2008. *Nature Geoscience,* **4**(3), 151-155. https://doi.org/10.1038/ngeo1062

Flanner, M. G., Zender, C. S., Hess, P. G., Mahowald, N. M., Painter, T. H., Ramanathan, V., & Rasch, P. J. (2009). Springtime warming and reduced snow cover from carbonaceous particles. *Atmospheric Chemistry and Physics,* **9**(7), 2481–2497. https://doi.org/10.5194/acp-9-2481-2009

Frei, A., Miller, J. A., & Robinson, D. A. (2003). Improved simulations of snow extent in the second phase of the Atmospheric Model Intercomparison Project (AMIP-2). *Journal of Geophysical Research: Atmospheres,* **108**, 4369–4384. https://doi.org/10.1029/2002JD003030

Furtado, J. C., Cohen, J. L., Butler, A. H., Riddle, E. E., & Kumar, A. (2015). Eurasian snow cover variability and links to winter climate in the CMIP5 models. *Climate Dynamics,* **45**(9), 2591-2605. https://doi.org/10.1007/s00382-015-2494-4

Groisman, P., Shugart, H., Kicklighter, D., Henebry, G., Tchebakova, N., Maksyutov, S., Monier, E., et al. (2017). Northern Eurasia future initiative (NEFI): facing the challenges and pathways of global change in the twenty-first century. *Progress in Earth and Planetary Science,* **4**(1), 1-48. https://doi.org/10.1186/s40645-017-0154-5

Gudmundsson, L. (2011). Large-scale hydrology in Europe: observed patterns and model performance. Norway. https://www.osti.gov/etdeweb/biblio/21573439

Guo, H., Bao, A., & Chen, T. (2021). Assessment of CMIP6 in simulating precipitation over arid Central Asia. *Atmospheric Research,* **252**, 105451. https://doi.org/10.1016/j.atmosres.2021.105451

Hall, A. (2004). The role of surface albedo feedback in climate. *Journal of Climate,* **17**(7), 1550-1568. https://doi.org/10.1175/1520-0442(2004)017<1550:TROSAF>2.0.CO;2

Hardiman, S. C., Kushner, P. J., & Cohen, J. (2008). Investigating the effect of fall Eurasian snow cover on winter climate in General Circulation Models. *Journal of Geophysical Research: Atmospheres,* **113**, D21123. https://doi.org/10.1029/2008JD010623

Harris, I., Osborn, T. J., Jones, P., & Lister, D. (2020). Version 4 of the CRU TS monthly high-resolution gridded multivariate climate dataset. *Scientific Data,* **7**(1), 1-18. https://doi.org/10.1038/s41597-020-0453-3

Henderson, G. R., Peings, Y., Furtado, J. C., & Kushner, P. J. (2018). Snow–atmosphere coupling in the Northern Hemisphere. *Nature Climate Change,* **8**(11), 954-963. https://doi.org/10.1038/s41558-018-0295-6

IPCC. 2013. Climate Change 2013: The Physical Science Basis. Contribution of Working Group I to the Fifth Assessment Report of the Intergovernmental Panel on Climate Change. In: Stocker, T. F., Qin, D., Plattner, G. K., Tignor, M., Allen, S. K., Boschung, J., Nauels. A., Xia, Y., et al. Atlas of Global and Regional Climate Projections: Cambridge University Press. 1311-1394.

Jiang, Z., Li, W., Xu, J., & Li, L. (2015). Extreme precipitation indices over China in CMIP5 models. Part I: Model evaluation. *Journal of Climate,* **28**(21), 8603–8619. https://doi.org/10.1175/JCLI-D-15-0099.1

Jin, Q., Wei, J., Lau, W. K. M., Pu, B., & Wang, C. (2021). Interactions of Asian mineral dust with Indian summer monsoon: Recent advances and challenges. *Earth-Science Reviews,* **215**, 103562. https://doi.org/10.1016/j.earscirev.2021.103562

Jones, P. W. (1999). First-and second-order conservative remapping schemes for grids in spherical coordinates. *Monthly Weather Review,* **127**(9), 2204-2210. https://doi.org/10.1175/1520-0493(1999)127<2204:FASOCR>2.0.CO;2

Kang, S., Zhang, Q., Qian, Y., Ji, Z., Li, C., Cong, Z., Zhang, Y., et al. (2019). Linking atmospheric pollution to cryospheric change in the Third Pole region: current progress and future prospects. *National Science Review,* **6**(4), 796-809. https://doi.org/10.1093/nsr/nwz031

Kannenberg, S. A., Maxwell, J. T., Pederson, N., D'Orangeville, L., Ficklin, D. L., Phillips, R. P. (2018). Drought legacies are dependent on water table depth, wood anatomy and drought timing across the eastern US. *Ecology Letters,* **22**(1), 119-127. https://doi.org/10.1111/ele.13173

Kouki, K., Räisänen, P., Luojus, K., Luomaranta, A., & Riihelä, A. (2021). Evaluation of Northern Hemisphere snow water equivalent in CMIP6 models with satellite-based SnowCCI data during 1982–2014. The Cryosphere, **2021**, 1-32. https://doi.org/10.5194/tc-2021-195

Kulinich, M., Fan, Y., Penev, S., Evans, J. P., & Olson, R. (2021). A Markov chain method for weighting climate model ensembles. *Geoscientific Model Development*, **14**(6), 3539-3551. https://doi.org/10.5194/gmd-14-3539-2021

Li, J., Huo, R., Chen, H., Zhao, Y., & Zhao, T. (2021). Comparative assessment and future prediction using CMIP6 and CMIP5 for annual precipitation and extreme precipitation simulation. *Frontiers in Earth Science,* **9**, 687976. https://doi.org/10.3389/feart.2021.687976

Li, Y., Wang, T., Zeng, Z., Peng, S., Lian, X., & Piao, S. (2016). Evaluating biases in simulated land surface albedo from CMIP5 global climate models. *Journal of Geophysical Research: Atmospheres,* **121**(11), 6178-6190. https://doi.org/10.1002/2016JD024774

Loranty, M. M., Berner, L. T., Goetz, S. J., Jin, Y., & Randerson, J. T. (2014). Vegetation controls on northern high latitude snow-albedo feedback: observations and CMIP5 model simulations. *Global Change Biology,* **20**(2), 594–606. https://doi.org/10.1111/gcb.12391

Lutz, A. F., Immerzeel, W. W., Siderius, C., Wijngaard, R. R., Nepal, S., Shrestha, A. B., Wester, P., & Biemans, H. (2022). South Asian agriculture increasingly dependent on meltwater and groundwater. *Nature Climate Change,* **12**, 566–573. https://doi.org/10.1038/s41558-022-01355-z

Mankin, J. S., & Diffenbaugh, N. S. (2015). Influence of temperature and precipitation variability on near-term snow trends. *Climate Dynamics,* **45**(3), 1099-1116. https://doi.org/10.1007/s00382-014-2357-4

Meinshausen, M., Smith, S. J., Calvin, K., Daniel, J. S., Kainuma, M. L. T., Lamarque, J. F., Matsumoto, K., et al. (2011). The RCP greenhouse gas concentrations and their extensions from 1765 to 2300. *Climatic change,* **109**(1), 213-241. https://doi.org/10.1007/s10584-011-0156-z

Meredith, M., Sommerkorn, M., Cassotta, S., Derksen, C., Ekaykin, A., Hollowed A., Kofinas, G., et al. (2019). Polar Regions. In: IPCC Special Report on the Ocean and Cryosphere in a Changing Climate.

Milly, P. C. D., & Dunne, K. A. (2020). Colorado River flow dwindles as warming-driven loss of reflective snow energizes evaporation. Science, **367**(6483), 1252-1255. https://doi.org/10.1126/science.aay9187

Mudryk, L., Derksen, C., Kushner, P. J., & Brown, R. (2015). Characterization of Northern Hemisphere snow water equivalent datasets, 1981–2010. *Journal of Climate,* **28**(20), 8037–8051, https://doi.org/10.1175/JCLI-D-15-0229.1

Mudryk, L., Kushner, P., Derksen, C., & Thackeray, C. (2017). Snow cover response to temperature in observational and climate model ensembles. *Geophysical Research Letters,* **44**(2), 919–926. https://doi.org/10.1002/2016GL071789

Mudryk, L., Santolaria-Otín, M., Krinner, G., Ménégoz, M., Derksen, C., Brutel-Vuilmet, C., Brady, M., & Essery, R. (2020). Historical Northern Hemisphere snow cover trends and projected changes in the CMIP6 multi-model ensemble. *The Cryosphere*, **14**(7), 2495-2514. https://doi.org/10.5194/tc-14-2495-2020

Pithan, F., & Mauritsen, T. (2014). Arctic amplification dominated by temperature feedbacks in contemporary climate models. *Nature geoscience,* **7**(3), 181-184. https://doi.org/10.1038/ngeo2071

Qu, X., & Hall, A. (2005). Surface contribution to planetary albedo variability in cryosphere regions. *Journal of Climate,* **18**(24), 5239-5252.

https://doi.org/10.1175/JCLI3555.1

Raftery, A. E., Gneiting, T., Balabdaoui, F., & Polakowski, M. (2005). Using Bayesian model averaging to calibrate forecast ensembles. *Monthly weather review,* **133**(5), 1155-1174. https://doi.org/10.1175/MWR2906.1

Robinson, D. A., Dewey, K. F., & Heim Jr, R. R. (1993). Global Snow Cover Monitoring: An Update. *Bulletin of the American Meteorological Society,* **74**(9), 1689-1696. https://doi.org/10.1175/1520-0477(1993)074<1689:GSCMAU>2.0.CO;2

Santolaria-Otín, M., & Zolina, O. (2020). Evaluation of snow cover and snow water equivalent in the continental Arctic in CMIP5 models. *Climate Dynamics,* **55**(11), 2993-3016. https://doi.org/10.1007/s00382-020-05434-9

Stewart, I. T., Cayan, D. R., & Dettinger, M. D. (2004). Changes in snowmelt runoff timing in western North America under a "business as usual" climate change scenario. *Climatic Change,* **62**(593), 217-232. https://doi.org/10.1023/B:CLIM.0000013702.22656.e8

Sturm, M., Goldstein, M. A., & Parr, C. (2017). Water and life from snow: A trillion dollar science question. *Water Resources Research,* **53**(5), 3534-3544. https://doi.org/10.1002/2017WR020840

Tang, Z., Wang, X., Wang, J., Wang, X., Li, H., & Jiang, Z. (2017). Spatiotemporal Variation of Snow Cover in Tianshan Mountains, Central Asia, Based on Cloud-Free MODIS Fractional Snow Cover Product, 2001–2015. *Remote Sensing,* **9**(10), 1045. https://doi.org/10.3390/rs9101045

Taylor, K. E. (2001). Summarizing multiple aspects of model performance in a single diagram. *Journal of Geophysical Research: Atmospheres,* **106**(D7), 7183-7192. https://doi.org/10.1029/2000JD900719

Taylor, K. E., Stouffer, R. J., & Meehl, G. A. (2021). An Overview of CMIP5 and the Experiment Design. *Bulletin of the American meteorological Society,* **93**(4), 485-498. https://doi.org/10.1175/BAMS-D-11-00094.1

Thackeray, C. W., Fletcher, C. G., & Derksen, C. (2015). Quantifying the skill of CMIP5 models in simulating seasonal albedo and snow cover evolution. *Journal of Geophysical Research: Atmospheres,* **120**(12), 5831–5849. https://doi.org/10.1002/2015JD023325

Thackeray, C. W., Fletcher C. G., Mudry, L. R., & Derksen, C. (2016). Quantifying the uncertainty in historical and future simulations of Northern Hemisphere spring snow cover. *Journal of Climate,* **29**(23), 8647-8663. https://doi.org/10.1175/JCLI-D-16-0341.1

Trenberth, K. E., & Fasullo, J. T. (2009). Global warming due to increasing absorbed solar radiation. *Geophysical Research Letters,* **36**(7), L07706. https://doi.org/10.1029/2009GL037527

van Kempen, G., van der Wiel, K., & Melsen, L. A. (2021). The impact of hydrological model structure on the simulation of extreme runoff

events. *Natural Hazards and Earth System Sciences,* **21**(3), 961-976. https://doi.org/10.5194/nhess-21-961-2021

Wang, L., Cole, J. N. S., Bartlett, P., Verseghy, D., Derksen, C., Brown, R., & von Salzen, K. (2016). Investigating the spread of surface albedo in snow covered forests in CMIP5 models. *Journal of Geophysical Research: Atmospheres,* **121**(3), 1104–1119. https://doi.org/10.1002/2015JD023824

Xia, K., & Wang, B. (2015). Evaluation and projection of snow cover fraction over Eurasia. *Climatic and Environmental Research (in Chinese),* **20**(1), 41-52. https://doi.org/10.3878/j.issn.1006-9585.2014.13126

Winton, M. (2006). Surface Albedo Feedback Estimates for the AR4 Climate Models. *Journal of Climate,* **19**(3), 359-365. https://doi.org/10.1175/JCLI3624.1

Wu, T., Yu, R., Lu, Y., Jie, W., Fang, Y., Zhang, L., Xin, X., et al. (2021). BCC-CSM2-HR: a high-resolution version of the Beijing climate center climate system model. *Geoscientific Model Development,* **14**(5), 2977–3006. https://doi.org/10.5194/gmd-14-2977-2021

Zhang, Y., You, Q., Chen, C., Ge, J., & Adnan, M. (2018). Evaluation of Downscaled CMIP5 coupled with VIC Model for Flash Drought simulation in a Humid Subtropical Basin, China. *Journal of Climate,* **31**(3), 1075–1090. https://doi.org/10.1175/JCLI-D-17-0378.1

Zhu, X., & Dong, W. (2013). Evaluation and Projection of Northern Hemisphere March-April Snow Covered Area Simulated by CMIP5 Coupled Climate Models. *Advances in Climate Change Research,* **9**(3), 173-180. https://doi.org/10.3969/j.issn.1673-1719.2013.03.003

Zhu, X., Lee, S. Y., Wen, X., Wei, Z., Ji, Z., Zheng, Z., & Dong, W. (2021). Historical evolution and future trend of Northern Hemisphere snow cover in CMIP5 and CMIP6 models. *Environmental Research Letters,* **16**(6), 065013. https://doi.org/10.1088/1748-9326/ac0662